Cell Reports

Article

Opposing roles of ZEB1 in the cytoplasm and nucleus control cytoskeletal assembly and YAP1 activity

Graphical abstract

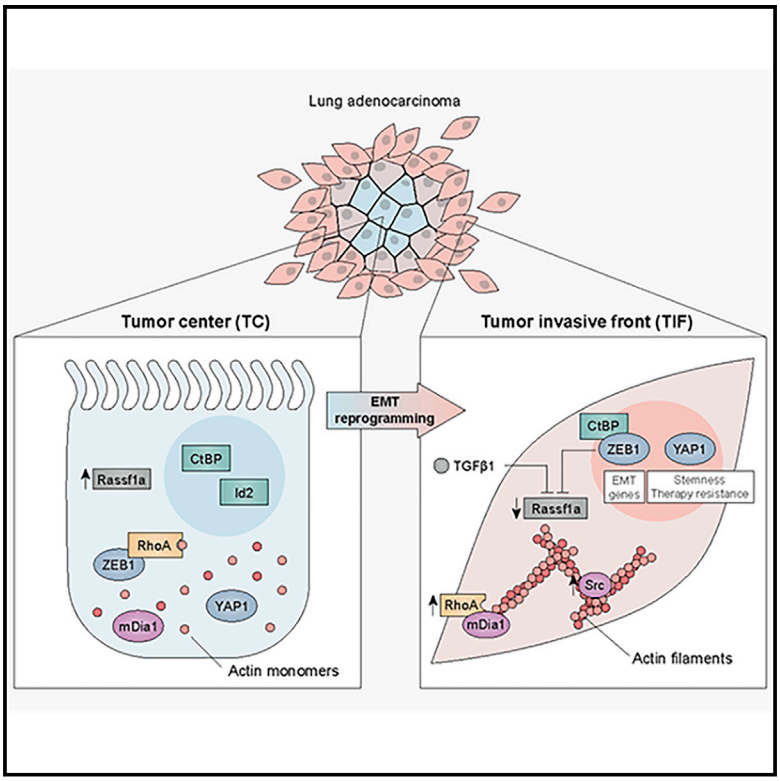

Highlights

- Cytoplasmic Zeb1 inhibits actin cytoskeleton assembly
- TGFb regulates Zeb1 nuclear transport
- A Zeb1 nuclear transport signature predicts LUAD outcome
- Zeb1 controls Yap1 nuclear transport

Authors

Yan Guo, Xiaoqin Lu, Yao Chen, ..., Antonio Postigo, Yongqing Liu, Douglas C. Dean

Correspondence

idib412@clinic.cat (A.P.), yongqing.liu@louisville.edu (Y.L.), douglas.dean@louisville.edu (D.C.D.)

In brief

Guo et al. show that Zeb1 cycles between the cytoplasm and nucleus in lung cancer, where it controls cytoskeleton assembly and Yap1 nuclear transport in the cytoplasm and initiates epithelial-mesenchymal transition gene expression as TGFB drives its transition to the nucleus.

Guo et al., 2022, Cell Reports *41*, 111452
October 4, 2022
https://doi.org/10.1016/j.celrep.2022.111452

CellPress

Cell Reports

CellPress
OPEN ACCESS

Article

Opposing roles of ZEB1 in the cytoplasm and nucleus control cytoskeletal assembly and YAP1 activity

Yan Guo,[1,4] Xiaoqin Lu,[1] Yao Chen,[1,5] Geoff Clark,[2] John Trent,[1] Miriam Cuatrecasas,[6] Douglas Emery,[1] Zhao-Hui Song,[2] Julia Chariker,[3] Eric Rouchka,[3] Antonio Postigo,[1,7,8,*] Yongqing Liu,[1,*] and Douglas C. Dean[1,9,*]

[1]Department of Medicine, Brown Cancer Center, University of Louisville Health Sciences Center, Louisville, KY 40202, USA
[2]Department of Pharmacology, Brown Cancer Center, University of Louisville Health Sciences Center, Louisville, KY 40202, USA
[3]Department of Computer Engineering and Computer Science, Brown Cancer Center, University of Louisville Health Sciences Center, Louisville, KY 40202, USA
[4]Department of Hematology, The First Affiliated Hospital of Shandong First Medical University, Jinan 250014, China
[5]Department of Ophthalmology, Xiangya Hospital of Central South University, Changsha, China
[6]Department of Pathology, Centro de Diagnóstico Biomédico (CDB) Hospital Clínic, University of Barcelona, 08036 Barcelona, Spain
[7]Group of Transcriptional Regulation of Gene Expression, IDIBAPS and University of Barcelona School of Medicine, 08036 Barcelona, Spain
[8]ICREA, 08010 Barcelona, Spain
[9]Lead contact
*Correspondence: idib412@clinic.cat (A.P.), yongqing.liu@louisville.edu (Y.L.), douglas.dean@louisville.edu (D.C.D.)
https://doi.org/10.1016/j.celrep.2022.111452

SUMMARY

Epithelial-mesenchymal transition (EMT) facilitates cancer invasion and is initiated by mesenchyme-driving transcription factors and actin cytoskeletal assembly. We show a cytoplasmic-to-nuclear transport gradient of the EMT transcription factor Zeb1 toward sites of invasion in lung adenocarcinoma (LUAD), driven by the EMT inducer Tgfb, which is expressed in M2 polarized macrophages. We show that Zeb1 binds free actin monomers and RhoA in the cytoplasm to inhibit actin polymerization, blocking cell migration and Yap1 nuclear transport. Tgfb causes turnover of the scaffold protein Rassf1a, which targets RhoA. Release of this RhoA inhibition in response to Tgfb overcomes Zeb1's block of cytoskeleton assembly and frees it for nuclear transport. A ZEB1 nuclear transport signature highlights EMT progression, identifies dedifferentiated invasive/metastatic human LUADs, and predicts survival. Blocking Zeb1 nuclear transport with a small molecule identified in this study inhibits cytoskeleton assembly, cell migration, Yap1 nuclear transport, EMT, and precancerous-to-malignant transition.

INTRODUCTION

Epithelial-mesenchymal transition (EMT) drives cancer cell invasion, leading to metastasis (Berenguer and Celià-Terrassa, 2021; Bracken and Goodall, 2022; Dongre and Weinberg, 2019; Gupta et al., 2021; Han et al., 2022; Lu and Kang, 2019; Meyer-Schaller et al., 2019; Moustakas and de Herreros, 2017). E box-binding transcription factors regulate epithelial versus mesenchymal gene expression in early EMT, and Zeb1 is key in initiating an EMT gene expression pattern in invading cancer cells by complexing with its co-repressor CtBP to repress epithelial genes while interacting with activated R-Smads on gene promoters to induce mesenchymal genes (Pastushenko et al., 2018; Postigo et al., 2003). *Zeb1* mutation or inhibition by the miR-200 family is sufficient to block EMT and invasion in genetically engineered mouse models (GEMMs) of K-Ras-initiated adenocarcinomas (Gregory et al., 2008; Krebs et al., 2017; Liu et al., 2014, 2018). Also early in EMT, monomeric G actin polymerizes into linear filamentous (F) actin (Pastushenko et al., 2018), with subsequent branching of F actin into a network that anchors cancer cell invasion. In late-stage EMT, the actin cytoskeleton interacts with myosin II to generate tension, which promotes nuclear transport of Yap1 (Lüönd et al., 2022; Moroishi et al., 2015; Pastushenko et al., 2018; Shreberk-Shaked and Oren, 2019). Yap1 and Zeb1 regulate cancer cell plasticity during invasion and metastasis (Moroishi et al., 2015; Wellner et al., 2009).

Tgfb is a key driver of cancer EMT (Batlle and Massagué, 2019; Derynck et al., 2021) that accumulates at the invasive tumor front (Huang et al., 2016). This signaling pathway can promote cytoskeleton assembly by causing Itch-mediated degradation of the cytoskeleton-associated protein Rassf1a (Pefani et al., 2016), which serves as a scaffold to bring Smurf1 to RhoA for its degradation (Lee et al., 2016). With diminished Rassf1a downstream of Tgfb, the level of RhoA increases, and it binds the Formin family member mDia1. The RhoA-mDia1complex then binds G actin and adds the monomers to the end of growing F actin (Narumiya et al., 2009; Otomo et al., 2005). As with RhoA, Rasssf1a also targets Src (Vlahov et al., 2015), and with loss of Rassf1a downstream of Tgfb, Src promotes activation of Arp2/3 to facilitate branching of F actin into a network (Tehrani et al., 2007). RhoA also activates ROCK to facilitate myosin II association with F actin, which forms a cytoskeletal network that anchors contractile force from cell-cell and cell-extracellular matrix contacts to drive Yap1 nuclear transport (Moroishi et al., 2015; Pastushenko et al., 2018; Shreberk-Shaked and

Oren, 2019; Zhang et al., 2021). Rassf1a-mediated targeting of RhoA and Src then inhibits cytoskeleton assembly as well as ROCK-dependent mechanical tension anchored in the actin cytoskeleton. Mutation or epigenetic deregulation of the genes controlling cytoskeleton assembly, *Rassf1a*, *RhoA*, and *Src*, is oncogenic and can drive EMT (Cortes et al., 2018; Grawenda and O'Neill, 2015; Hsu et al., 2020). Tgfb-initiated early EMT requires RhoA and Formin activity, demonstrating its dependence on actin polymerization (Bhowmick et al., 2001; Rana et al., 2018). How onset of actin cytoskeleton assembly in the cytoplasm might be linked to a Zeb1-initiated EMT gene expression pattern in the nucleus is unclear.

Here we show that Zeb1 shuttles between the cytoplasm and the nucleus in mouse and human lung cancer. In the central tumor, where cells maintain an epithelial expression pattern, cytoplasmic Zeb1 inhibits actin cytoskeletal assembly, cell migration, and Yap1 nuclear transport. In response to Tgfb expressed by M2 polarized macrophage cell at sites of invasion, Zeb1 is transported to the nucleus, relieving cytoskeletal inhibition and initiating EMT gene expression. We analyzed the pathway through which Zeb1 inhibits cytoskeleton assembly and how it is transported from the cytoplasm to the nucleus and show that a gene expression signature representing these pathways reflects EMT progression and identifies tumors with epithelial dedifferentiation and repression of tumor suppressors and cyclin-dependent kinase inhibitors that block the cell cycle.

RESULTS

Zeb1 transitions from the cytoplasm in the central tumor to the nucleus at Tgfb1-rich sites of invasion

EMT reprogramming of cancer cells at the invasive front of carcinomas, including GEMM of K-Ras-driven lung adenocarcinoma (LUAD), is classically characterized by loss of epithelial markers (e.g., E-cadherin [Cdh1]) and induction of mesenchymal markers (e.g., vimentin [Vim]) (Figure 1A; Liu et al., 2018; Zhang and Weinberg, 2018). Tgfb classically triggers EMT; it accumulates at the invasive front of tumors (Huang and Blobe, 2016; Figure 1B) and is a negative predictor of lung cancer outcome (Li et al., 2019). Immune cells are rich sources of Tgfb, and serum Tgfb facilitates metastasis of circulating tumor cells (Grainger et al., 2000; Huang et al., 2016). Tgfb1 immunostaining was evident in and around blood vessels in the tumor periphery and around airways, where blood vessels are closely associated (Figures 1C and 1D). We used single-cell RNA sequencing (scRNA-seq) of human LUAD to investigate the cell source of TGFB family members. We found that only TGFB1 was expressed (Figure 1E). It was expressed primarily by CD45 (PTPRC)+ immune cells, with COL1A1+ tumor-associated fibroblasts expressing relatively little TGFB1 (Figure 1E). We then examined expression of immune cell markers. Only a few CD3+ T cells were evident, and they clustered with tumor cells and did not express TGFB1 (Figure 1E). NOS2+ M1 polarized macrophages were not evident, but CD163+ M2 macrophages were abundant and comprised most of the CD45+ cells in the tumors; they are the primary source of TGFB1 (Figure 1E).

We found Zeb1 accumulated in the nucleus of cells at the invasive front of K-Ras-initiated mouse LUAD, and it was nuclear in cells invading airways; similar nuclear expression of ZEB1 was evident at the invasive front of *K-RAS* mutant human LUAD (Figure 1F–1W). However, immunostaining for Zeb1 in the central region of human and mouse tumors, where tumor cells retained expression of the epithelial marker E-cadherin, revealed that Zeb1 was primarily cytoplasmic, where it co-localized with the cytoskeletal regulatory protein RhoA, and a transitional zone between cytoplasmic and nuclear localization was evident approaching the invasive margin of the tumors (Figures 1F–1W). These results show that Zeb1 translocates in a gradient fashion from the cytoplasm in the central tumor to the nucleus at the invasive front and as cells invade airways in Tgfb1-rich environments.

Tgfb1 promotes actin cytoskeleton assembly and Zeb1 and Yap1 nuclear translocation

Immunostaining of primary cell cultures from a GEMM of K-Ras-initiated LUAD (Ahn et al., 2012; Liu et al., 2018) demonstrated a mixture of cytoplasmic and nuclear localization of Zeb1 (Figure 2A). Mixed expression of E-cadherin and Vim suggested that cells had initiated a partial EMT (Figure 2B). As with Zeb1, Yap1 showed a mixture of cytoplasmic and nuclear immunostaining in the cells (Figure 1C). As expected, Tgfb1 treatment caused increased Vim and decreased E-cadherin, indicative of EMT progression, and also promoted nuclear translocation of Zeb1 and Yap1 (Figures 2D–2F). Similar results were seen with cells derived from K-RAS mutant human LUAD (Figure 3). Early EMT is also characterized by polymerization of monomeric G actin into linear F actin, which, in turn, assembles into a branched network that anchors cell shape changes mediating invasion and contractile tension, facilitating Yap1 nuclear transport in late-stage EMT. Phalloidin staining of F actin showed that Tgfb1 increased the number of these filaments, and it caused an increase in filament length, with filaments spanning the cell in the x-y dimension as well as the z dimension, reflecting cell thickness (Figures 2G–2L). This increased F actin cytoskeleton assembly is consistent with Tgfb1 promotion of Yap1 nuclear transport.

We fractionated cells into three cellular compartments: Gapdh-rich soluble cytoplasm, histone H3-rich nucleus, and Vim-rich cytoskeleton (Figure 2M). In untreated cells, Zeb1 was associated primarily with the cytoskeleton, consistent with our findings in the central tumor, where Zeb1 co-localized with the cytoskeletal regulatory protein RhoA (Figures 1J–1L). Also consistent with immunostaining results, Tgfb1 treatment caused Zeb1 nuclear translocation.

RASSF1A regulates cytoskeleton assembly, EMT, and nuclear translocation of Zeb1 and Yap1

Rassf1a is a scaffold protein that inhibits cytoskeleton assembly, and it is targeted for destruction by the E3 ubiquitin ligase Itch (Pefani et al., 2016). Itch is recruited to the Tgfb receptor, where it causes degradation of co-recruited Rassf1a in response to Tgfb (Pefani et al., 2016). Based on these findings, it seemed likely that loss of Rassf1a downstream of Tgfb1 is responsible for enhancing cytoskeleton assembly in LUAD cells. As with primary mouse LUAD cells, Tgfb1 initiated an early EMT gene expression pattern, F actin assembly, and nuclear translocation of ZEB1 and YAP1 in human LUAD cells (Figures 3A and 3B). As with Tgfb1 treatment, shRNA knockdown of RASSF1A in these cells

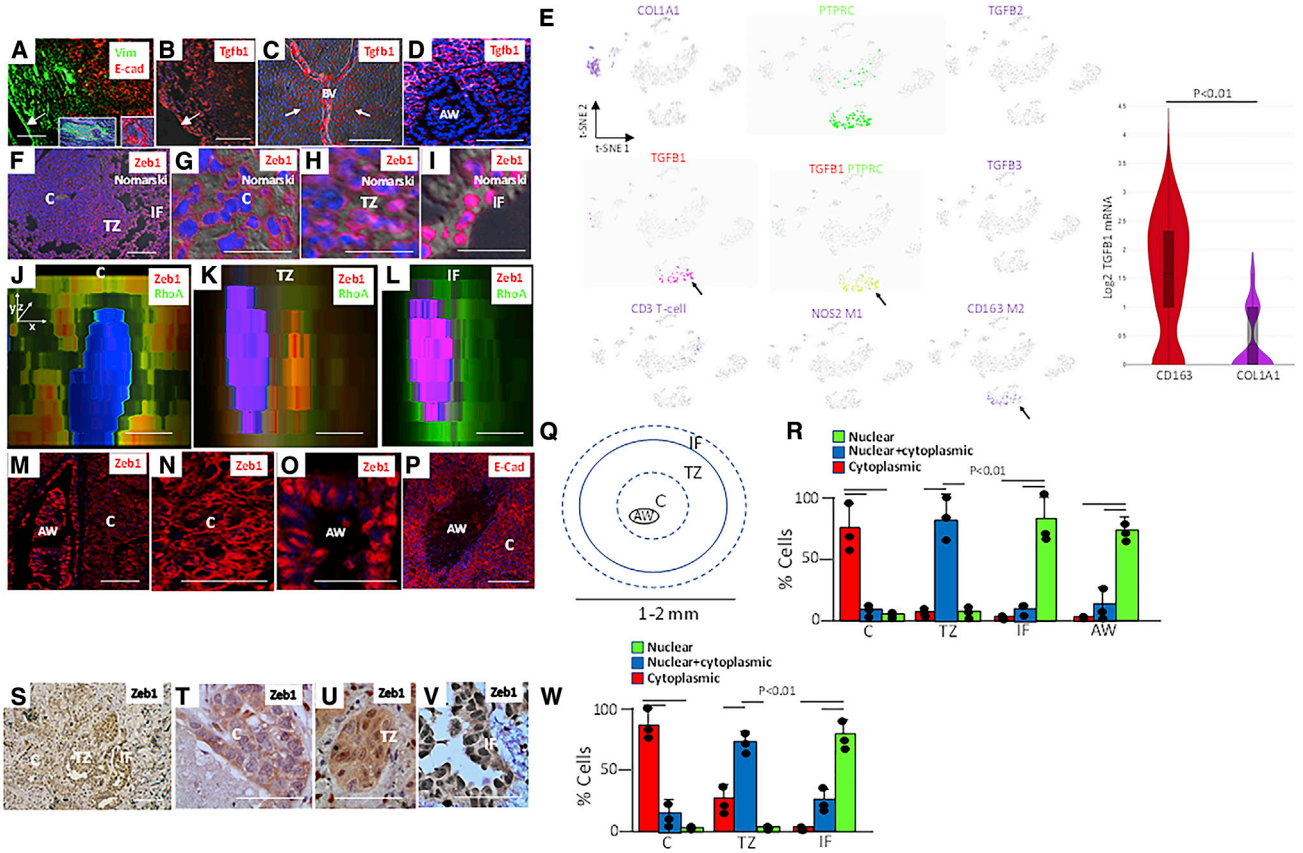

Figure 1. Zeb1 transitions from the cytoplasm in the central tumor to the nucleus at Tgfb1-rich sites of invasion

(A) Immunostaining of a mutant K-Ras-driven mouse LUAD at P220 for Vim and E-cadherin (E-Cad). The arrow shows the tumor edge. Insets show higher-power views of individual Vim+ and E-Cad+ cells.

(B) Tgfb1 accumulates with Vim at the invasive front of mouse LUAD. As in (A), immunostaining is shown of a tumor at P220. The arrow indicates the tumor edge.

(C) A blood vessel (BV) containing Tgfb1+ cells is shown. Arrows show Tgfb1 immunostaining surrounding the BV, indicating that Tgfb1-expressing cells are moving from the BV into the surrounding tumor.

(D) BVs run alongside airways (AWs) in the lungs, where they branch with the AWs. Note Tgfb1-immunostaining in the region surrounding the AWs.

(E) t-SNE1 (t-distributed stochastic neighbor embedding) versus t-SNE2 projection of scRNA-seq of K-RAS mutant human LUAD. Only TGFB1 mRNA is expressed, and it is enriched in PTPRC (CD45)+, CD163+ M2 polarized tumor macrophages. Log2 TBFB1 mRNA expression is compared in COL1A1+ tumor-associated fibroblasts and CD163+ M2 tumor macrophages.

(F–I) Zeb1 is cytoplasmic in the central tumor (C) and transitions to the nucleus at the invasive front (IF) of mouse LUAD. There is a transition zone (TZ) where Zeb1 shows a mixture of cytoplasmic and nuclear immunostaining between the C and the IF.

(J–L) High-power cut 3D confocal z stack images of cells from (G)–(I). Cytoplasmic Zeb1 co-localizes with the cytoskeletal regulatory protein RhoA.

(M–P) Zeb1 shows a similar cytoplasmic-to-nuclear transition as cells in the C as tumor cells invade AWs.

(Q) Diagram of tumors, showing sites of cell counting.

(R) Nuclear versus cytoplasmic distribution of Zeb1 in tumor regions illustrated in (Q). Fifty cells in the C, TZ, IF, and sites of AW invasion were counted in tumors in three different mice.

(S–V) Immunostaining showing Zeb1 cytoplasm-to-nuclear transition moving from the C to the IF of human *K-RAS* mutant LUAD.

(W) Results from (S)–(V) are quantified.

Scale bars represent 100 μm (A–D, F, M, P, and S–V), 50 μm (G–I, N, and O), and 5 μm (J–L). Error bars are standard deviations.

(Ahmed-Choudhury et al., 2005; Harrell Stewart et al., 2020) led to an increase in the number and length of actin filaments (Figures 3A–3D). With this increase in cytoskeleton assembly, ZEB1 and YAP1 translocated to the nucleus to initiate EMT, as assessed by induction of VIM and repression of E-cadherin (Figures 3A–3D). Tgfb1 treatment did not enhance the effect of RASSF1A knockdown on EMT gene expression or nuclear translocation of ZEB1 and YAP1 (Figure 3D), consistent with RASSF1A acting downstream of Tgfb1, as reported previously (Pefani et al., 2016). Supporting these immunostaining results, western blot analysis showed that Tgfb1 and RASSF1A knockdown triggered YAP1 translocation from the cytoplasm to the nucleus (Figure 3E).

Mutation of *Rassf1a* drives Zeb1 and Yap1 nuclear transport throughout lung tumors

To test a role for Rassf1a in nuclear transport of Zeb1 and Yap1 *in vivo*, GEMM K-Ras mice were crossed into a *Rassf1a* heterozygous background (Ahmed-Choudhury et al., 2005). Figures 4A and 4A′ show H&E staining of lung tumors. Immunostaining for Zeb1 and Yap1 was used to follow the subcellular localization of the

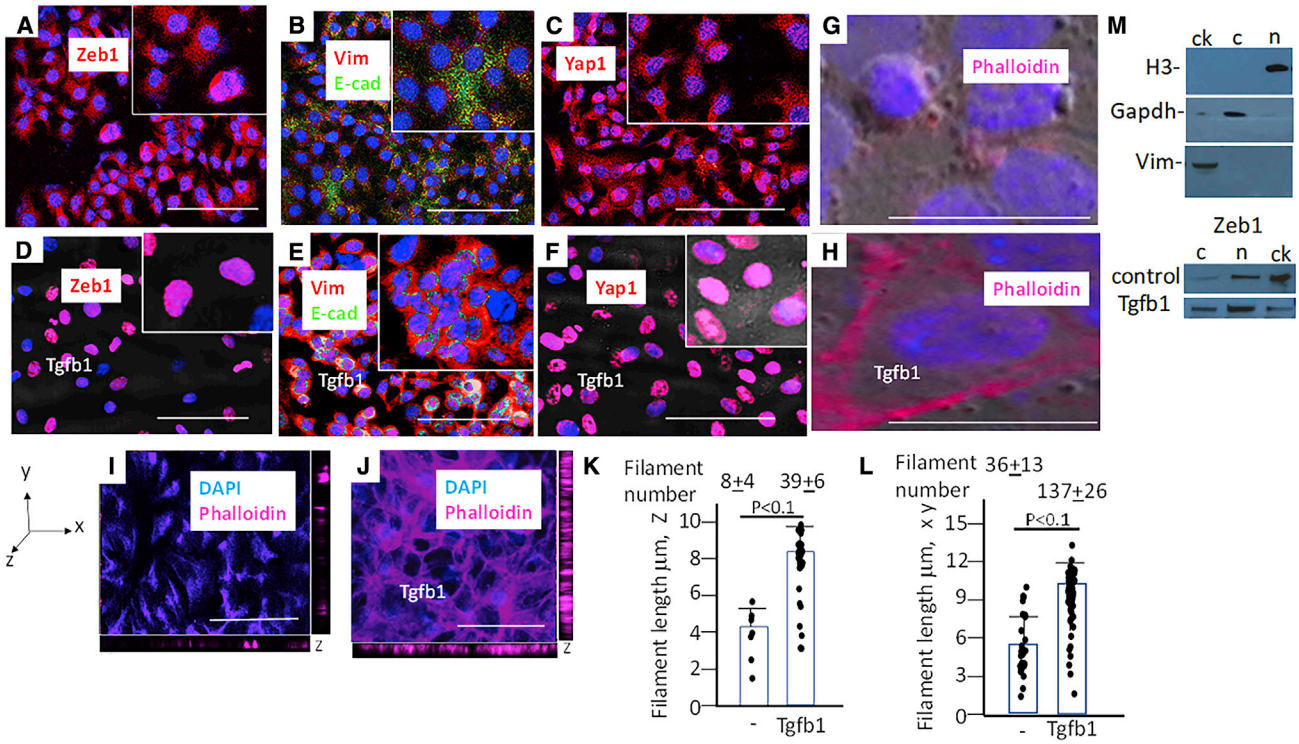

Figure 2. Tgfb1 drives EMT, F actin assembly and elongation, and Zeb1 and Yap1 nuclear localization in primary cultures of mouse LUAD cells

(A) Immunostaining for Zeb1 shows a mixture of cytoplasmic and nuclear localization in primary cultures of mouse LUAD cells.

(B) These cells also show a mixture of Vim and E-Cad immunostaining, demonstrating partial EMT.

(C) Like Zeb1, Yap1 immunostaining shows a mixture of cytoplasmic and nuclear localization.

(D) Tgfb1 treatment drives nuclear localization of Zeb1.

(E) Tgfb1 treatment (5 ng/mL for 24 h) induced Vim and diminished E-Cad immunostaining, indicative of EMT progression.

(F) Tgfb1 promotes Yap1 nuclear localization.

(G–L) Tgfb1 treatment increases Phalloidin-staining F actin. Phalloidin+ actin filaments were visualized in x-y and z dimensions in control and Tgfb1-treated cells. The number of F actin polymers was counted in the x-y and z dimensions of merged confocal z stacks in 20× microscopic views of confluent cells using cut views as in Figures 1J–1L. Fifty cells were counted. Polymer length in the x-y and z dimensions was measured by switching to a high-power view (40×). Cut views were used to count the number and length of filaments in the z dimension. Confluent cells on tissue culture plates were approximately 15 μm in thickness (z dimension). Error bars indicate standard deviation.

(M) Histone H3, Gapdh, and Vim were used as markers of nucleus (n), soluble cytoplasm (c), and cytoskeleton (ck) compartments in cell extracts, respectively (STAR Methods). A western blot of the compartments is shown. Tgfb1 treatment moves Zeb1 from the ck fraction to the n fraction.

Scale bars represent 50 μm (A–F and I–J) and 15 μm (G and H). Results are representative of at least three independent experiments.

proteins in these tumors (Figures 4B–4E). As with K-Ras-driven LUAD in a *Rassf1a*$^{+/+}$ background (Figures 1F–1R), Zeb1 was nuclear at the invasive tumor front and in cells invading surrounding lung parenchyma in *Rassf1a*$^{+/-}$ tumors (Figures 2B, 2D, and 2E). Similarly, Yap1 was nuclear at these sites (Figures 4C–4E). However, Zeb1 and Yap1 were nuclear at the center of Rassf1a-deficient lung tumors (Figures 4B–4E). We suggest that Tgfb1 at the tumor edge is targeting Rassf1a, promoting nuclear localization of Zeb1 and Yap1 in invading cells. With diminished Rassf1a after mutation, this pathway is short circuited, causing nuclear translocation of the transcription factors even in the center of the tumor, where Tgfb1 is low.

In a feedforward loop, Zeb1 binds the *Rassf1a* promoter and represses its expression

Inspection of the *Rassf1a* promoter region revealed consensus E box binding sites for Zeb1 (Figure 4F), raising the possibility that nuclear transport of Zeb1 might regulate Rassf1a expression. Knockdown of Zeb1 increased Rassf1a mRNA, whereas overexpression of Zeb1 decreased Rassf1a mRNA (Figures 4G and 4H). Chromatin immunoprecipitation assays demonstrated Zeb1 binding to the *Rassf1a* promoter *in vivo* (Figure 4I), and we concluded that initial nuclear transport of Zeb1 leads to a feedforward loop where repression of *Rassf1a* promotes cytoskeleton assembly and, in turn, Zeb1 nuclear transport.

RhoA and Formin activity is required for Tgfb1 and RASSF1A knockdown to initiate EMT, F actin assembly, and Zeb1 and Yap1 nuclear transport

Next, we used inhibitors of components important in F actin assembly to evaluate their role in Tgfb1-induced filament formation (Figures 5A–5G). RhoA inhibition blocked Tgfb1-induced F actin number and length (Figures 5A, 5B, 5F, and 5G). Likewise, Formin inhibition (aimed at targeting the Formin family member

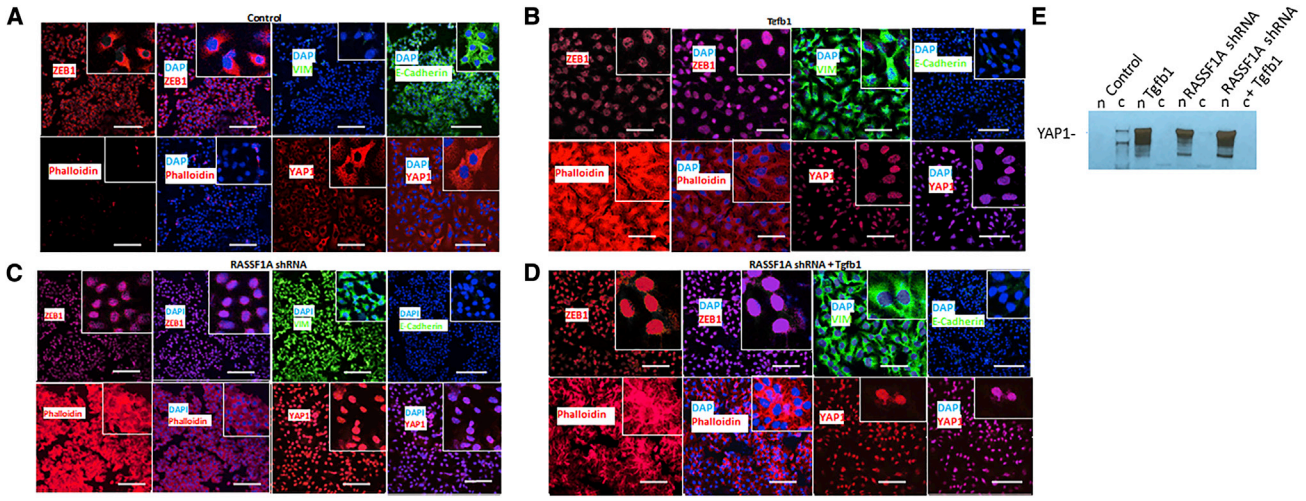

Figure 3. Tgfb1 treatment or RASSF1A knockdown promotes EMT, F actin assembly, and nuclear translocation of ZEB1 and YAP1

Immunostaining showing Tgfb1 treatment or RASSF1A knockdown (Harrell Stewart et al., 2020; Schmidt et al., 2018) in human LUAD cells (NCL-H1437).

(A) Immunostaining shows high E-Cad and low VIM, suggesting that the cells have not initiated EMT. The cells also show cytoplasmic Zeb1 and Yap1 and little Phalloidin+ F actin.

(B) As with mouse LUAD cells (Figure 2), Tgfb1 treatment of human LUAD cells caused induction of VIM and repression of E-Cad, indicative of EMT onset, assembly of Phalloidin+ F actin, and nuclear translocation of Zeb1 and Yap1.

(C) Like Tgfb1 treatment, RASSF1A knockdown caused EMT, F actin assembly, and nuclear translocation of Zeb1 and Yap1.

(D) Combining Tgfb1 and RASSF1A knockdown did not produce an additive effect consistent with Tgfb and RASSF1A acting in same pathway.

(E) Western blot showing that Tgfb1 treatment or RASSF1A knockdown promotes Yap1 translocation from the c to the n.

Scale bars represent 50 μm.

mDia1) also blocked F actin (Figures 5A, 5C, 5F, and 5G). RhoA and Formin inhibition also blocked F actin assembly in response to knockdown of RASSF1A (Figures 5F and 5G). Our results support a RhoA-mDia1 complex driving F actin assembly downstream of Tgfb1-RASSF1A. Consistent with diminished cytoskeleton assembly, RhoA or Formin inhibition blocked Yap1 nuclear translocation (Figures 5A–5C). RhoA and Formin inhibition also prevented the EMT gene expression pattern induced by Tgfb1 (Figures 5A–5C). Likely accounting for this failure in early EMT gene expression, RhoA or Formin inhibition blocked Tgfb1-induced nuclear transport of Zeb1 (Figures 5A–5C). These results raised the possibility that, as with Yap1, Tgfb1-RASSF1A-mediated actin cytoskeletal assembly might be regulating Zeb1 nuclear translocation.

Src activity is required downstream of Tgfb1-RASSF1A for F actin extension and Zeb1 and Yap1 nuclear transport

Rassf1a not only facilitates Itch-mediated degradation of RhoA, it also inhibits Src, which phosphorylates Cortactin to promote Arp2/3-mediated F actin branching (Tehrani et al., 2007; Vlahov et al., 2015). Src inhibition also blocked Tgfb1-and RASSF1A knockdown-induced Zeb1 and Yap1 nuclear translocation (Figures 5A and 5D). Next, we evaluated the effect of Src inhibition on F actin formation in x-y and z dimensions in the cell. Inhibition of Src did not affect the number of actin filaments in the planar x-y dimension or the perpendicular z dimension, but the length of these filaments was significantly decreased in both dimensions (Figures 5F and 5G). These shortened actin filaments are consistent with Src inhibition reducing F actin extension/branching. We concluded that Zeb1 nuclear translocation is not simply dependent on initiation of F actin assembly but on the subsequent Src-dependent extension/branching of these filaments.

ROCK activity is required for nuclear translocation of Yap1 but not Zeb1

Inhibition of ROCK did not affect Tgfb1 or RASSF1A knockdown-initiated F actin initiation or extension (Figures 5A, 5E, 5F, and 5G). ROCK inhibition did not reverse the early EMT gene expression pattern initiated by Tgfb1 (Figures 5A and 5E). Consistent with maintenance of this EMT expression pattern, ROCK inhibition did not prevent Zeb1 nuclear transport in response to Tgfb1 or Rassf1a knockdown (Figures 5A and 5E). However, in contrast to Zeb1, ROCK inhibition prevented Yap1 nuclear transport in response to Tgfb1 (Figures 5A and 5E). We concluded that actin polymerization driven by RhoA and Src downstream of Tgfb1 is promoting Zeb1 nuclear localization and, thus, early EMT gene expression, but ROCK-dependent cytoskeletal tension is not required. Although Yap1 nuclear transport also requires actin cytoskeletal assembly, its nuclear transport is distinct from Zeb1 in that it requires subsequent ROCK-dependent tension anchored by this cytoskeleton. These results demonstrate onset of EMT, as evidenced by repression of E-cadherin and induction of Vim, in the absence of nuclear Yap1.

Zeb1 binds RhoA and G actin and inhibits RhoA-mDia1 complex formation

Consistent with Rassf1a targeting RhoA downstream of Tgfb1, RhoA levels increased after Tgfb1 treatment or RASSF1A

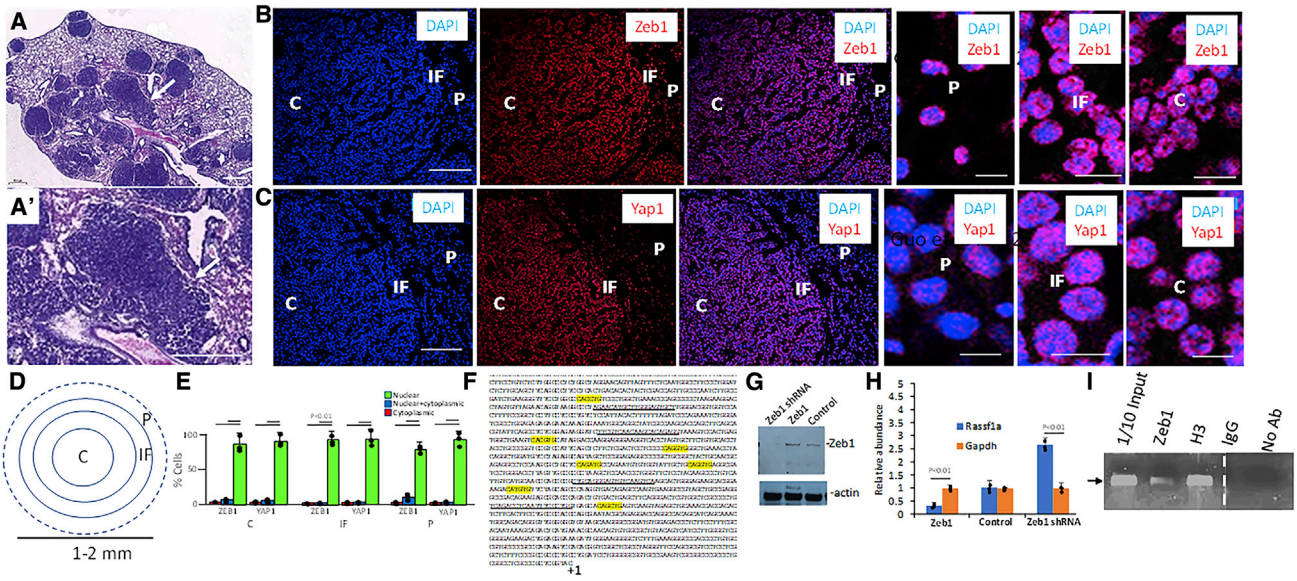

Figure 4. *Rassf1a* mutation promotes Zeb1 and Yap1 nuclear translocation throughout lung tumors, and nuclear Zeb1 represses *Rassf1a*

(A and A′) Mice that express doxycycline-inducible *K-Ras4b* ^{G12D} in lung ATII cells were crossed with *Rassf1a* knockout mice to generate *K-Ras4b* ^{G12D} x *Rassf1a*$^{+/-}$ mice. Animals approximately 4 months of age were fed doxycycline chow for 3 months, and tumors were assessed by H&E staining. Arrows show the same position.

(B and C) Immunostaining for Zeb1 and Yap1 is shown in the C at the IF and in surrounding lung parenchyma (P).

(D) Diagram of tumors, showing sites of cell counting.

(E) Cells were counted for nuclear versus cytoplasmic immunostaining of Zeb1 and Yap1 in tumor regions illustrated in (D). Scale bars represent 100 μm (10 μm in higher-power images in B and C). Three different tumors in two different mice were evaluated.

(F) Sequence of the mouse *Rassf1a* gene promoter region, showing multiple consensus E box binding sites for Zeb1 (yellow). Most E boxes are conserved in the human sequence. Bars indicate primers used for the chromatin immunoprecipitation (ChIP) assays in (I).

(G) Western blot showing shRNA knockdown or overexpression of Zeb1 in primary mouse LUAD cells (Liu et al., 2014).

(H) Real-time PCR analysis showing that Zeb1 is repressing Rassf1a mRNA.

(I) ChIP assay showing that Zeb1 binds the *Rassf1a* promoter *in vivo*. "H3" indicates immunoprecipitation with a positive control histone antibody and negative controls with pre-immune immunoglobulin G (IgG) and no antibody. The dashed line indicates controls from a different region of the same gel.

Scale bars represent 50 μm (A), 100 μm (A′), 50 μm (low-power images in B and C) and 10 μm (higher-power images). Error bars are standard deviations.

knockdown (Figure 6A). Because RhoA and Formin activity and, in turn, F actin assembly are linked to Zeb1 nuclear transport, we wondered whether Zeb1 might interact with RhoA, mDia1, or actin in the cytoplasm. We then immunoprecipitated Zeb1 from cell extracts and examined associated proteins by western blot. RhoA and G actin co-precipitated with Zeb1, but mDia1 was notably absent from the complex (Figures 5H and 5I). These results suggest that interaction of Zeb1 with RhoA and actin is displacing mDia1, implying that cytoplasmic Zeb1 is actively inhibiting polymerization of monomeric G actin into F actin.

Tgfb1 treatment switches Zeb1 from a RhoA/G actin complex to a CtBP complex

Tgfb1 treatment or RASSF1A knockdown induced the level of RhoA and caused an increase in F actin with a corresponding decrease in soluble G actin (Figure 5H). We concluded that elevated RhoA in response to Tgfb1 drives G actin into F actin, overcoming inhibition by cytoplasmic Zeb1. Despite this increase in RhoA, Zeb1-RhoA diminished under these conditions (Figure 5I), suggesting that the complex is dependent upon G actin, and as G-actin diminishes with its incorporation into F actin in response to Tgfb, Zeb1-RhoA is lost. Concomitant with loss of RhoA and G actin binding in the presence of Tgfb1, Zeb1 formed a complex with its nuclear co-repressor, CtBP (Figure 5I). Neither RhoA nor G actin was present in the Zeb1-CtBP complex (Figure 5I). These results suggest that Zeb1 binds CtBP when its complex with RhoA and G actin dissociates in response to Tgfb1 treatment.

Cytoplasmic Zeb1 inhibits F actin number and length

Consistent with CtBP interaction transporting Zeb1 to the nucleus, knockdown of CtBP1/2 led to accumulation of Zeb1 in the cytoplasm of primary mouse LUAD cells, and it prevented Tgfb1 treatment from promoting Zeb1 nuclear localization (Figures 6A–6D). Concomitantly, the number and length of actin filaments was reduced, providing evidence that cytoplasmic Zeb1 is inhibiting F actin (Figures 6A–6D).

Attempts by our group and others to overexpress Zeb1 in a variety of cells have led to cells stably expressing no more than a 2-fold increase over baseline (Figure 4G). These results suggest that most cells do not tolerate high levels of Zeb1 overexpression. Based on our findings with CtBP knockdown, we hypothesized that overexpression of Zeb1 is leading to a block in cytoskeletal assembly. Because actin polymerization plays a key role in spindle assembly, a complete block would be expected to inhibit mitosis. F actin sequesters Trim21 to prevent its

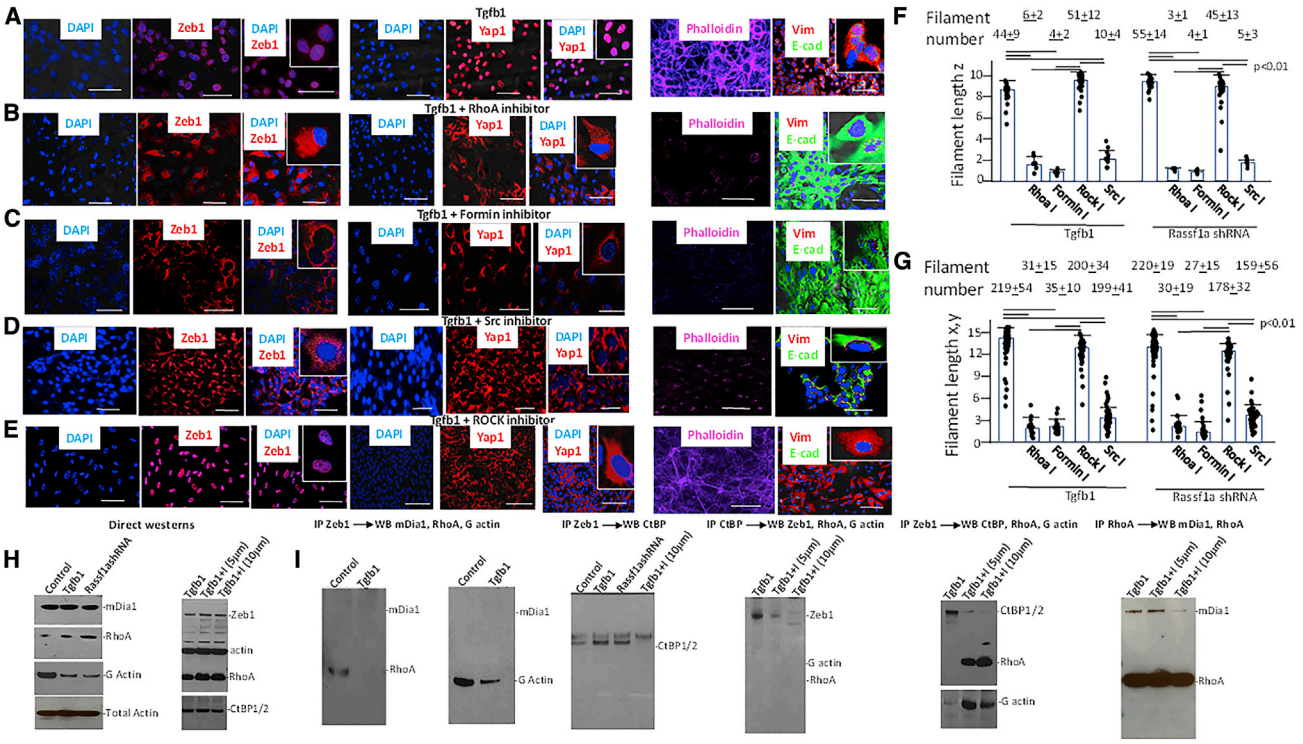

Figure 5. RhoA, Formin, and Src inhibition blocks Tgfb1-induced EMT, cytoplasmic-to-nuclear translocation of Zeb1 and Yap1, and F actin assembly in LUAD cells

Zeb1 binds RhoA and G actin, displaying mDia1. Tgfb1 or Rassf1a knockdown eliminates Zeb1 binding to RhoA, shifting Zeb1 into a complex with CtBP. A small-molecule Zeb1-CtBP interaction inhibitor promotes a complex between Zeb1 and RhoA and G actin.

(A) Control showing that Tgfb1 treatment induces Vim and represses E-Cad, indicative of EMT progression; drives nuclear translocation of Zeb1 and Yap1; and promotes Phalloidin+ F actin assembly.

(B) Treatment of the cells with a RhoA inhibitor prevents Tgfb1-induced EMT, F actin assembly, and nuclear translocation of Zeb1 and Yap1.

(C) Likewise, Formin inhibition prevents Tgfb1-induced EMT, F actin assembly, and nuclear Zeb1 and Yap1.

(D) Src inhibition blocks Tgfb1-induced EMT, elongation of F actin, and Zeb1 and Yap1 nuclear translocation.

(E) ROCK inhibition failed to prevent Tgfb1-induced EMT, F actin assembly, or Zeb1 nuclear localization, but it blocked nuclear translocation of Yap1. Scale bars represent 50 μm. Results are representative of at least three independent experiments. Inhibitor treatment is described in the STAR Methods.

(F and G) Effects of RhoA, Formin, Src, and ROCK inhibition on Phalloidin+ F actin assembly was quantified in the z (reflecting cell thickness) and x-y dimensions as in Figures 2K and 2L and STAR Methods. The number of Phalloidin+ filaments, with standard deviation, is shown above each bar. Error bars are standard deviations.

(H) Direct western blots of primary mouse LUAD cells treated as indicated. "I" indicates a small-molecule Zeb1-CtBP inhibitor (Figure S1).

(I) Cell extracts were immunoprecipitated with antibodies to Zeb1, CtBP, or RhoA, and proteins were western blotted as illustrated above the gels. Results are representative of three independent experiments.

degradation of PFK and Hif1a; thus, inhibition of F actin might also release Trim21 to block glycolysis (Chen et al., 2021; Park et al., 2020). Primary mouse LUAD cells were examined after infection with a Zeb1-expressing lentivirus that co-expresses GFP from an internal ribosome entry site in the 3′ untranslated region of Zeb1 mRNA (Liu et al., 2014). GFP+ cells showed elevated immunostaining for ZEB1, with the increase in Zeb1 being primarily cytoplasmic, implying that overexpression is overwhelming nuclear transport capacity (Figures 6E and 6F). This increase in cytoplasmic Zeb1 led to loss of F actin, and the cells rounded up and failed to proliferate (Figures 6E–6G). We conclude that cytoplasmic Zeb1 accumulating after overexpression is blocking cytoskeletal assembly and, in turn, proliferation. Two different approaches leading to cytoplasmic accumulation of Zeb1 provide evidence showing that Zeb1 is inhibiting F actin.

Identification of a small-molecule inhibitor of the Zeb1-CtBP complex

We wondered whether a small molecule could be identified that selectively targets the Zeb1-CtBP interaction to modulate subcellular localization of Zeb1. CtBP interacts with multiple binding partners via a surface groove or a hydrophobic cleft (Nardini et al., 2003). Some proteins, including Zeb1 and CoRest, interact with the cleft through a PLDLS-like motif (Postigo and Dean, 1999; Postigo et al., 2003; Wang et al., 2007; Zhang et al., 2002; Zhao et al., 2009). These PLDLS motifs vary in sequence, and some cleft binders lack a PLDLS motif. CtBP forms an NADH/NAD+ driven dimer with dehydrogenase activity, which is required for its co-repressor function (Kuppuswamy et al., 2008). Dimerization causes a conformational narrowing of the cleft, which is required for interaction of most cleft binders

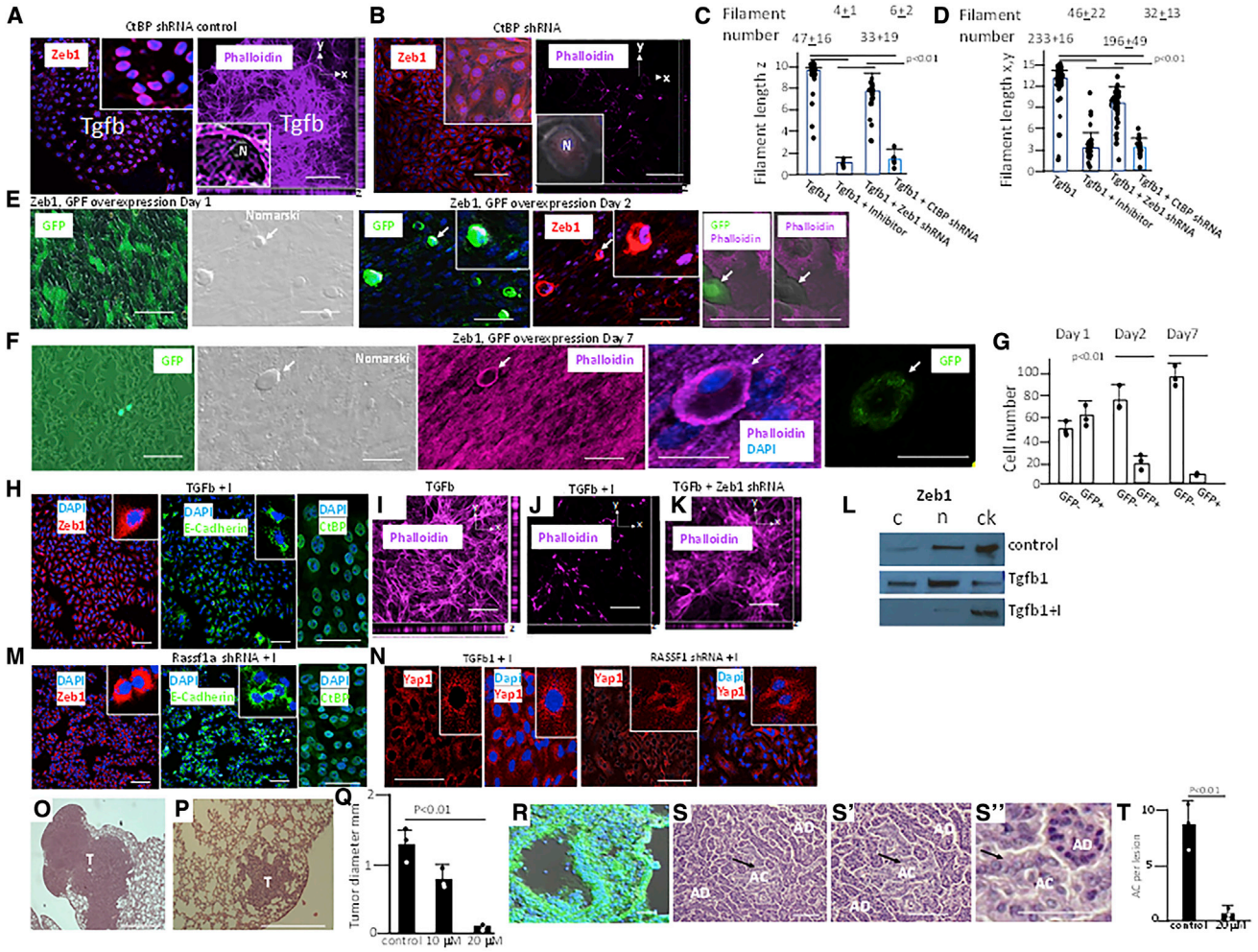

Figure 6. Knockdown of CtBP, overexpression of Zeb1, and blocking Zeb1-CtBP with a small-molecule inhibitor prevents Tgfb1 or RASSF1A knockdown from driving EMT, nuclear translocation of Zeb1 and Yap1, F actin assembly, and precancerous-to-malignant transition in K-Ras-initiated lung cancer

(A and B) Lentivirus shRNA knockdown of CtBP1/2 (Figure S4) causes cytoplasmic retention of Zeb1 and loss of F actin assembly in Tgfb1-treated cells.

(C and D) Phalloidin+ filaments were quantified in the x-y and z dimensions as in Figures 2K and 2L (STAR Methods). The number of Phalloidin+ filaments, with standard deviation, is shown above each bar.

(E and F) Lentivirus overexpression of Zeb1, with GPF co-expressed from an IRES in Zeb1 mRNA, leads to accumulation of cytoplasmic Zeb1, loss of phalloidin+ actin filaments, and cell rounding. Cells are shown at days 1, 2, and 7 after infection. Arrows show the same position.

(G) GPF+ and GFP− cells were counted in 20× views on the indicated days after infection.

(H) Treatment with the Zeb1-CtBP inhibitor (I) (Figure S1) at 5 μm prevents Tgfb1-induced repression of E-Cad and nuclear translocation of Zeb1, but it does not affect nuclear transport of CtBP.

(I–K) Zeb1-CtBP inhibition blocks Tgfb1-induced F actin assembly, but shRNA knockdown of Zeb1 (Figure 4G) only modestly affects this assembly. Results are quantified in (C) and (D).

(L) Western blot showing that I blocks Tgfb1-induced Zeb1 nuclear transport, leading to Zeb1 association with the ck. See also Figure 2M and STAR Methods.

(M and N) Zeb1-CtBP inhibition prevents Tgfb1 treatment and RASSF1A knockdown from repressing E-Cad and Zeb1 and Yap1 nuclear translocation. Scale bars represent 50 μm. Results are representative of at least three independent experiments.

(O and P) Precancerous adenomas (ADs) appear around P120 in the K-Ras-initiated model of lung LUAD in Figure 1 (Johnson et al., 2001; Liu et al., 2014, 2018). Then foci of adenocarcinoma (AC) begin to appear within these ADs around P150, and they expand in number and size.

(Q) We delivered 100 μL of Zeb1-CtBP I in PBS, or PBS only as a control, intratracheally twice a week beginning at P120 in three WT and K-Ras mutant mice as we described previously (Liu et al., 2014), and lungs were evaluated at P200. All mice survived. The I diminished tumor diameter in the K-Ras mutant mice.

(R) As a delivery efficiency control, 100 μL of lentivirus expressing GFP was delivered intratracheally (Liu et al., 2014).

(S–S″) Example of an AC focus developing within an AD. Arrows show the same position.

(T) AC foci per lesion were counted in three different mice. Standard deviations are shown.

(Kumar et al., 2002; Kuppuswamy et al., 2008). A dimer-dependent loop at the edge of the catalytic site appears to interact with the PLDLS motif, also potentially explaining the dependence of dimer formation on partner binding. Two cleft binders, Zeb1 and HDAC2, interact with CtBP independent of dimerization (Kumar et al., 2002; Kuppuswamy et al., 2008). The dehydrogenase catalytic site forms a cavity at the entrance to the cleft. As expected, binding of partners to the cleft does not affect CtBP dehydrogenase activity, suggesting functional distinction of the catalytic site and adjacent partner binding within the cleft. However, mutations in the catalytic cavity inhibit interaction of most cleft binders, demonstrating their dependence on residues within this adjacent cavity (Kumar et al., 2002; Kuppuswamy et al., 2008). Again, binding of Zeb1 and HDAC2 is unaffected by catalytic cavity mutations (Kuppuswamy et al., 2008). These findings point to structural differences in binding of Zeb1 and HDAC2 to the CtBP cleft compared with other cleft binders. The PLDLS-like motifs in Zeb1 are not obviously distinguishable from those in other cleft binders. Although HDAC2 seems to parallel Zeb1 in binding assays to CtBP mutants, it interacts with the cleft via a non-PLDLS motif (Kuppuswamy et al., 2008). We then concluded that the context of a PLDLS motif or other binding motif within a given protein likely shapes distinct contact points with the CtBP cleft. Although Zeb1 and CoRest bind CtBP in a PLDLS-dependent fashion, CoRest is a necessary co-factor for Zeb1 repression, and Zeb1 bound to target genes forms a complex with CtBP bound to CoRest, implying independent binding sites on CtBP for Zeb1 and CoRest (Wang et al., 2007). We reasoned that analysis of a series of small molecules resembling different regions of the larger CtBP cleft might identify a selective inhibitor of Zeb1-CtBP interaction.

Using molecular screening of the crystal structure of the CtBP cleft and a PLDLS-like sequence, we searched ~25,000,000 compounds for small molecules that would occupy the larger CtBP cleft (Figure S1). We identified 27 candidate compounds. Compounds were initially evaluated for solubility and cell toxicity in culture. Then, because we hypothesized that the context of a PLDLS motif within a given protein dictates its contact points with CtBP, we evaluated candidates for their ability to inhibit interaction of full-length proteins with CtBP *in vivo* using co-immunoprecipitation assays at micromolar concentration (Figure S2). In addition to Zeb1, we evaluated binding of CoRest, which mirrors other PLDLS motif proteins in its dependence on dimerization and the dehydrogenase binding cavity, and HDAC2, which parallels Zeb1 in its interaction with CtBP mutants but utilizes a non-PLDLS motif for CtBP binding (Figure S2). One compound (N-{3-[4-(2,5-dimethylphenyl) piperazin-1-yl] propyl-1-(6-methyl-1H-1,3-benzodiazol-2-yl) piperidine-3-carboxamide) was identified that efficiently blocked Zeb1-CtBP interaction but did not disrupt interaction of CoRest or HDAC2 with CtBP (Figures S1 and S2), and this compound was selected for further study.

Inhibition of Zeb1-CtBP interaction blocks Tgfb1 and RASSF1A knockdown-induced Zeb1 and Yap1 nuclear transport, EMT, and cell migration

Treatment of primary cultures of K-Ras-initiated mouse LUAD cells with the Zeb1-CtBP interaction inhibitor prevented Tgfb1-initiated E-cadherin repression and inhibited Zeb1-dependent cell migration (Figure S3). Overexpression of Zeb1 in the cells overcame these effects of the inhibitor, supporting the notion that effects of the inhibitor are a result of targeting Zeb1 interaction with CtBP (Figure S3). Although this overexpression is only ~2-fold, it is functionally significant in that it promotes invasion and metastasis when the primary LUAD cells are transplanted back into the mouse lung (Yang et al., 2014). As with knockdown of CtBP, Zeb1-CtBP interaction inhibition caused retention of Zeb1 and Yap1 in the cytoplasm in Tgfb1-treated or RASSF1a knockdown cells, prevented repression of E-Cadherin, and disrupted F actin (Figures 6H–6N). CtBP still translocated to the nucleus when the Zeb1-CtBP interaction was disrupted (Figure 6H). Taken together with the CtBP knockdown experiments above, these results indicate that binding to CtBP is required for Zeb1 nuclear translocation but that this interaction is not required for CtBP nuclear transport.

Binding of Zeb1 to CtBP prevents its binding to RhoA and G actin

Because the Zeb1-CtBP complex was blocked in cells treated with Tgfb1 or with RASSF1A knockdown, a Zeb1 complex containing RhoA and G actin increased (Figure 5I). Concomitantly, G actin levels increased, reflecting its decreased incorporation into F actin (Figure 5I). Immunoprecipitation of RhoA showed interaction with mDia1, and this interaction was inhibited when Zeb1 was released from Zeb1-CtBP, freeing it to form a complex with RhoA (Figure 5I). These results show that the inhibitor does not block a Zeb1-RhoA/G actin complex, demonstrating independent binding sites on Zeb1 for CtBP and RhoA/G-actin. However, the two Zeb1 complexes are mutually exclusive. It is possible that cytoskeletal localization of Zeb1, via a RhoA/G-actin complex, might sequester Zeb1 away from CtBP. Alternatively, a relatively bulky RhoA/G-actin complex might sterically inhibit CtBP interaction. Nevertheless, there appears to be an equilibrium between the Zeb1 complexes, and a shift toward RhoA/G-actin, displacing mDia1 as the CtBP interaction is inhibited, is sufficient to block Tgfb1-induced F actin. Despite co-immunoprecipitation of RhoA with Zeb1, we did not detect Zeb1 with RhoA immunoprecipitation, which might indicate that RhoA antibody binding is sterically blocking Zeb1 binding.

Cytoplasmic retention of Zeb1 is functionally distinct from Zeb1 loss

To compare cytoplasmic retention of Zeb1 versus overall loss of Zeb1, cells where Zeb1 was knocked down with lentivirus shRNA (Figure 4G) were compared with cells with Zeb1-CtBP interaction inhibition or CtBP knockdown, where nuclear Zeb1 was eliminated, but cytoplasmic Zeb1 was enriched (Figures 6D, 6H, 6I–6K, 6M, and 6N). Zeb1 knockdown or Zeb1-CtBP inhibition reversed E-cadherin repression by Tgfb1 or RASSF1A knockdown, consistent with nuclear Zeb1 being required to drive this repression (Figure 6H and 6M); however, the number and length of actin filaments was significantly less when Zeb1 accumulated in the cytoplasm after Zeb1-CtBP inhibition or CtBP knockdown compared with Zeb1 knockdown (Figures 6A–6D and 6I–6K). These results emphasize the biological role of cytoplasmic Zeb1 in inhibition of F actin and highlight the difference between

retention of Zeb1 in the cytoplasm relative to overall loss in Zeb1 expression via knockdown or gene mutation.

Zeb1 inhibition blocks precancerous-to-malignant transition in lung cancer

We delivered 100 μL of the Zeb1-CtBP interaction inhibitor intratracheally twice a week beginning at post-natal day 120 (P120) into eight wild-type (WT) and eight K-Ras mutants, and lungs were evaluated at P200. As a control, PBS was delivered to eight K-Ras mutant mice. All animals survived. No histological changes were evident in the WT mice. Similar to *Zeb1* mutation or Zeb1 shRNA knockdown, the inhibitor diminished tumor diameter in the K-Ras mutant mice (Figures 6O–6Q). As a delivery efficiency control, 100 μL of lentivirus expressing GFP was delivered intratracheally (Figure 6R).

Precancerous adenomas first appear around P120 in this GEMM (Johnson et al., 2001; Liu et al., 2014). Foci of adenocarcinoma begin to appear within these adenomas around P150, and they expand in number and size by P200. As a mesenchymal marker, Zeb1 is not expressed in normal lung epithelium, nor is it expressed in adenomas, but it is induced as foci of adenocarcinoma develop (Liu et al., 2018). Mutation or knockdown of Zeb1 blocked this adenoma-to-adenocarcinoma transition (Liu et al., 2018). Therefore, we counted foci of adenocarcinoma in lung tumors and found that, as with mutation or knockdown, Zeb1-CtBP interaction inhibition blocked focus formation, preventing the important precancerous-to-malignant transition (Figures 6S and 6T).

A ZEB1 nuclear transport signature is linked to *K-RAS* and *p53* mutation, EMT progression, cancer cell dedifferentiation, invasion/metastasis, and LUAD survival

We analyzed components regulating ZEB1 nuclear transport and outcome measures of this transport in human LUAD. Rassf1a mediates Tgfb-initiated nuclear transport of Zeb1, and Zeb1, in turn, represses *Rassf1a*. Consistent with our findings in primary cell culture, RASSF1A mRNA in tumors in affected individuals correlated positively with expression of mRNA for the epithelial specification gene *CDH1* (encoding E-cadherin) and negatively with the mesenchymal gene *VIM* (Figure 7A), linking downregulation of RASSF1A mRNA to tumor EMT. Along with Zeb1, other E box-binding transcription factors modulate EMT (Dongre and Weinberg, 2019). Id2 interacts with these E box-binding transcription factors, blocking their activity (Gervasi et al., 2012). Zeb1 directly represses Id2 in a Tgfb1-dependent fashion, releasing inhibition of these other EMT transcription factors to launch an EMT gene expression pattern (Chen et al., 2017). As an initial sensor of ZEB1 nuclear translocation, repression of ID2 mRNA correlated with induction of the ZEB1 target gene VIM and low levels of RASSF1A mRNA in tumors in affected individuals (Figure 7A). We found that cohorts of individuals with low RASSF1A or ID2 mRNA (the lower 50% of tumors) had poorer survival (Figure 7B). High ID2 expression has been correlated previously with improved survival in LUAD (Lu et al., 2020). A combined RASSF1A/ID2 mRNA-low signature (reflecting ZEB1 nuclear localization and function) was compared with a high signature, consistent with cytoplasmic retention of ZEB1. The combined low signature was synergistic in predicting negative outcome (Figure 7B). Next, we compared oncogenic mutations in *EGFR*, *K-RAS*, and in *p53* in the high- versus low-expression signatures. We found that *EGFR* mutations were more common in the high group that showed a more positive outcome (Figure 7C). In contrast, *K-RAS* and *p53* mutations were more prominent in the low group with a poorer outcome (Figure 7C). K-RAS-activating mutation causes ERK-catalyzed inactivating phosphorylation of MCRIP1, which otherwise inhibits ZEB1 interaction with CtBP (Ichikawa et al., 2015). Taken together with our findings, these results point to K-RAS mutation having an active role in driving ZEB1 nuclear transport by promoting ZEB1-CtBP. p53 induces mir-200 family members that target ZEB1 mRNA, leading to its down regulation, linking *p53* mutation to elevated ZEB1 (Kim et al., 2011). K-RAS and p53 mutations promote bronchial epithelial cell engagement of EMT in response to Tgfb1 (Larsen et al., 2016).

Heatmaps comparing mRNA expression in normal lungs with high- and low-signature tumor groups showed that normal lung samples clustered with the high group (Figures 7D and 7E). Although portions of the high- and low-group tumors clustered together in an intermediate expression pattern, most tumors in the low group, emphasizing ZEB1 nuclear transport and EMT, clustered separately (Figure 7E). Progression of EMT has been shown to play a critical role in tumor properties, including plasticity, invasion, and metastasis (Lüönd et al., 2021; Pastushenko et al., 2018, 2021), and the GO analysis in Table S1 demonstrates induction of multiple EMT regulators.

We wanted to determine whether LUAD tumor clustering into low, intermediate, and high groups reflected graded EMT in response to progression of the ZEB1 nuclear transport signature. CDH2 expression marks late-stage EMT whereas Tenacin C (TNC), ITGAV, and ITGB3 have been shown to highlight partial EMT (Lüönd et al., 2021; Pastushenko et al., 2018, 2021). We found induction of CDH2 in low-signature tumors whereas TNC, ITGAV, and ITGB3 were expressed in the intermediate tumors and diminished in the high-signature tumors or in normal lung (Figure 7F). These results demonstrate EMT progression in human LUAD linked to the level of a ZEB1 nuclear transport signature.

When average mRNA expression was compared in the high- and low-signature groups, more than 400 genes showed an at least 3-fold reduction in expression in the low signature, whereas less than 50 genes showed induction. These results are consistent with gene repression being a prominent feature of the low signature, indicative of nuclear ZEB1-CtBP activity. Lung epithelium-specific genes were repressed with onset of EMT in the low signature (Figure 7G). GO (gene ontology) analysis comparison of low- and high-signature tumors identified multiple pathways and genes involved in onset of EMT, actin and actin filament binding, and lung function (Table S1). Specifically, markers for lung ATII cells, the cell of origin for human and GEMM of K-Ras-initiated LUAD, were downregulated in the low versus high signature (Table S2). Pathological scoring of the tumors showed that most high-group tumors were well differentiated (epithelial-like), whereas low-group tumors were poorly differentiated (mesenchymal-like) (Figure 7C). GO analysis also showed downregulation of multiple cyclin-dependent kinase inhibitors in the low group, which normally block the cell cycle, and

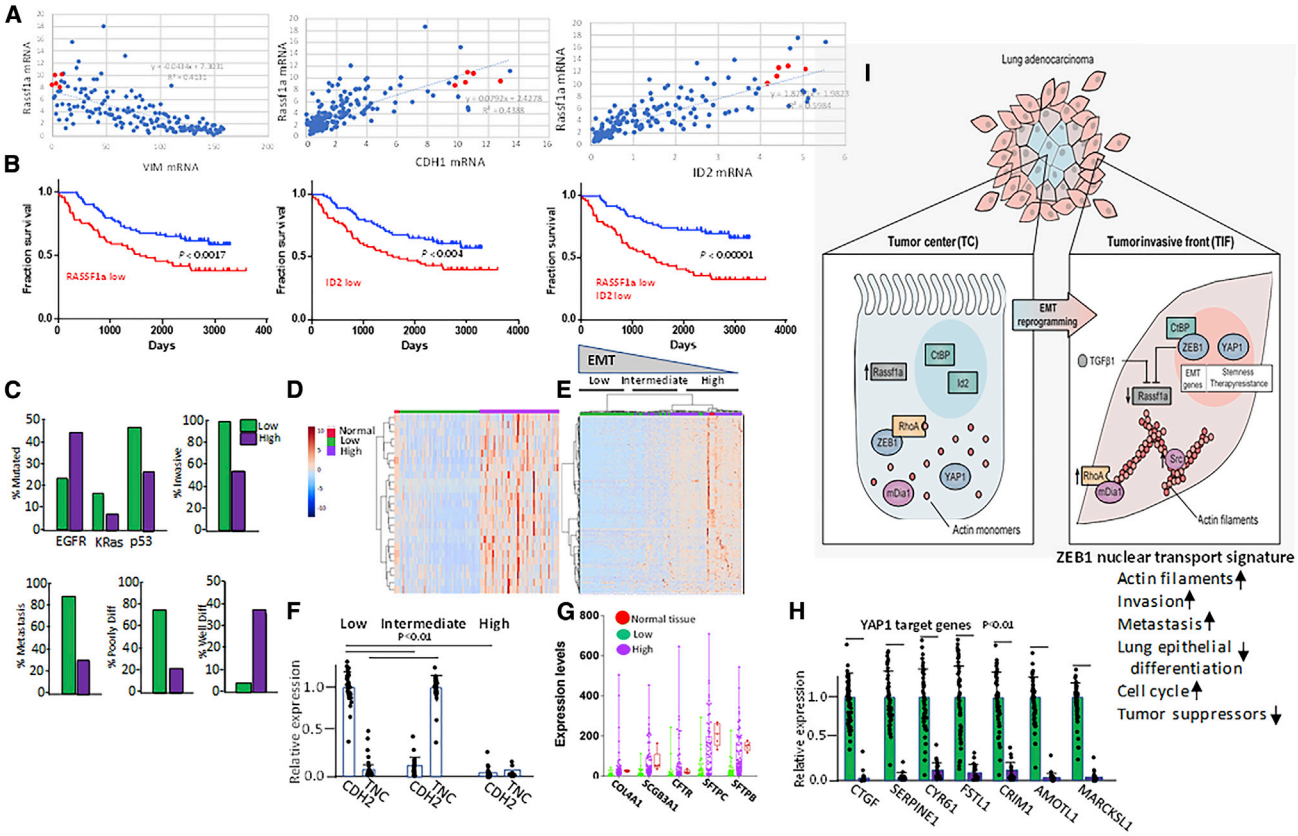

Figure 7. A Zeb1 nuclear transport signature highlights EMT progression, K-RAS and P53 mutation, lung epithelial dedifferentiation, and invasion and metastasis, and it predicts LUAD survival

We utilized RASSF1A and ID2 mRNA repression as a signature of ZEB1 nuclear transport in human LUAD (see text).

(A) Downregulation of RASSF1A mRNA in human lung LUADs correlates with downregulation of ID2 mRNA and with an EMT mRNA expression pattern. Red circles correspond to normal lung tissue.

(B) Survival curves show that low levels of RASSF1A or ID2 mRNA are negative factors in LUAD survival. We designated tumors in the lower half of RASSF1A ID2 mRNA expression as displaying a signature of ZEB1 nuclear transport, and in 124 tumors it identified individuals with a poor outcome.

(C) *EGFR* mutations are more frequent in the RASSF1A ID2-high signature, whereas K-RAS and P53 mutation are enriched in the RASSF1A ID2-low tumors. The RASSF1A ID2-low signature identifies poorly differentiated, invasive, and metastatic tumors.

(D and E) Heatmaps show downregulation of numerous genes in the low signature versus the high signature or normal lung tissue. Hierarchical clustering of tumors on the right shows that normal lung tissue samples cluster with the high signature, some low- and high-signature tumors cluster together in an intermediate pattern, but most low-signature tumors segregate separately and are highlighted by a reduction in gene expression.

(F) Expression of EMT progression markers CDH2 (end-stage EMT) and TNC (partial EMT) (Lüönd et al., 2021) shows that the ZEB1 nuclear transport signature "low RASSF1A/ID2" highlights EMT progression in human LUAD tumors in (E).

(G) Downregulation of genes important for epithelial differentiation and specifically for lung function and maintenance of club and AT2 cells in low-signature tumors. $p < 0.05$ low versus high signature. See also Figures S5 and S6.

(H) Supporting the dependence of YAP1 activity on ZEB1 nuclear transport, the ZEB1 nuclear transport signature identified tumors showing induction of YAP1 target genes. Error bars are standard deviations.

(I) Model depicting opposing ZEB1 activities in the c and n (light blue). See text for discussion. TC, tumor center; TIF, tumor IF. Up arrows denote increased expression and down arrows decreased expression.

downregulation of tumor suppressors (Table S1). We also found gene expression changes in pathways linked to cell adhesion and migration, indicative of EMT (Table S1). Accordingly, all low-group tumors were invasive, and 90% of them metastasized to other organs (Figure 7C).

Consistent with the linkage we demonstrate between ZEB1 and YAP1 nuclear transport, known targets of YAP1 were selectively induced in the low-signature tumors, reflecting ZEB1 nuclear transport (Figure 7H).

DISCUSSION

We provide evidence showing that Zeb1 has opposing roles in cancer EMT. In the cytoplasm of cancer cells, Zeb1 blocks F actin assembly, which is required for cell migration/invasion. In response to Tgfb1 concentrated at sites of invasion, Zeb1 forms a complex with its co-repressor CtBP, reversing its inhibition of F actin and causing its transported to the nucleus to initiate an EMT gene expression pattern (Figure 7I). Zeb1's cytoplasmic

block of F actin prevents assembly of a cytoskeletal mechanical anchor required for Yap1 nuclear transport (Figure 7I), causing Yap1 nuclear translocation to be dependent on Zeb1 nuclear transport.

Repression of the EMT transcription factor inhibitor ID2 and the cytoskeletal inhibitor RASSF1A forms a signature of ZEB1 nuclear transport in human LUAD. Id2 is a marker of lung distal tip progenitors that give rise to differentiated lung epithelial cell types (Rawlins et al., 2009). Tgfb-initiated repression of Id2 deregulates this differentiation process as well as lung epithelial regeneration (Chen et al., 2017; Kiyokawa et al., 2020), implying that repression of ID2 and the accompanying onset of EMT are responsible, at least in part, for lung epithelial cell dedifferentiation seen in tumors displaying a nuclear ZEB1 signature. Accordingly, AT2 specification transcription factors, including ETV5 and NKX2-1, are repressed in tumors displaying a ZEB1 nuclear transport signature, as is GRHL2, which interacts with NKX2-1 to control differentiation of lung progenitors into specialized epithelium (Varma et al., 2012). Nuclear ZEB1 directly represses *GRHL2* (Cieply et al., 2013), suggesting that its targeting of the NKX2-1/GRHL2 loop is reversing epithelial differentiation in human LUAD cells.

Our findings point to a feedforward ZEB1/RASSF1A loop where RASSF1A controls ZEB1 nuclear transport and cytoskeleton assembly, and nuclear ZEB1, in turn, represses RASSF1A to promote cytoskeleton assembly and ZEB1 nuclear transport.

We link Tgfb1 to nuclear transport of ZEB1 and YAP1 and show that it is expressed primarily by M2 polarized tumor macrophages. We have recently demonstrated that Zeb1+ tumor cells in LUAD are adjacent to M2 macrophages concentrated at the tumor invasive front and sites of tumor cell invasion into large airways (Guo et al., 2021). At these sites, CD47 induced by Zeb1 on tumor cells interacts with Sirpa on macrophages to promote M2 polarization, which, in turn, inhibits T cell migration and activation in tumors.

Limitations of the study

Our conclusions regarding cytoplasmic versus nuclear functions for Zeb1 are limited to K-Ras-driven lung cancer. Zeb1-CtBP interaction inhibition is being utilized as a complementary tool to demonstrate that interaction with CtBP is required for Zeb1 nuclear transport and to assess the role of cytoplasmic Zeb1 in regulation of cytoskeletal assembly and Yap1 nuclear transport. Zeb1 is not expressed in normal adult lung, and its induction is confined to disease and injury (Liu et al., 2018; https://www.proteinatlas.org/). It will be important to assess the potential for inhibiting Zeb1 in tumor models.

STAR★METHODS

Detailed methods are provided in the online version of this paper and include the following:

- KEY RESOURCES TABLE
- RESOURCE AVAILABILITY
  - Lead contact
  - Materials availability
  - Data and code availability
- EXPERIMENTAL MODEL AND SUBJECT DETAILS
  - Mice
  - Human studies
  - Cell lines, primary culture
- METHOD DETAILS
  - Cell fractionation
  - F actin number and length
  - RhoA, Formin, Src and ROCK inhibition
  - RNA extraction, real-time PCR and ChIP assays
  - shRNA knockdown
  - Immunostaining
  - Identification of a novel Zeb1-CtBP binding inhibitor
  - Characterization of a RASSF1A, ID2 signature in human LUAD
- QUANTIFICATION AND STATISTICAL ANALYSIS

SUPPLEMENTAL INFORMATION

Supplemental information can be found online at https://doi.org/10.1016/j.celrep.2022.111452.

ACKNOWLEDGMENTS

We thank Jon Kurie for primary mouse LUAD cells and Douglas Darling for the Zeb1 antibody. This study was supported by NIH grants (to Y.L. and D.C.D.) and AECC (PROYE19040POST), the Olga Torres Foundation, AVON-SAU, and MICINN (PID2020-116338RB-I00, co-financed by the EU ERDF) (to A.P.).

AUTHOR CONTRIBUTIONS

Y.G. performed immunostaining. X.L. bred mice, collected tumors, and maintained cells in culture. Y.L. and Y.C. performed real-time PCR and ChIP assays. X.L. and Z.-H.S. performed coIP assays and western blots. D.E. generated heatmaps and evaluated human expression signatures. M.C. evaluated tumor pathology. G.C. provided K-Ras × *Rassf1a* mutant mice and RASSF1A knockdown human lung cancer cells. J.T. performed virtual screening for Zeb1-CtBP inhibitors. D.C.D., Y.G., Y.L., and A.P. planned experiments, analyzed results, and wrote the manuscript.

DECLARATION OF INTERESTS

The authors declare no competing interests.

Received: March 21, 2022
Revised: July 12, 2022
Accepted: September 14, 2022
Published: October 4, 2022

REFERENCES

Ahmed-Choudhury, J., Agathanggelou, A., Fenton, S.L., Ricketts, C., Clark, G.J., Maher, E.R., and Latif, F. (2005). Transcriptional regulation of cyclin A2 by RASSF1A through the enhanced binding of p120E4F to the cyclin A2 promoter. Cancer Res. *65*, 2690–2697.

Ahn, Y.H., Gibbons, D.L., Chakravarti, D., Creighton, C.J., Rizvi, Z.H., Adams, H.P., Pertsemlidis, A., Gregory, P.A., Wright, J.A., Goodall, G.J., et al. (2012). ZEB1 drives prometastatic actin cytoskeletal remodeling by downregulating miR-34a expression. J. Clin. Invest. *122*, 3170–3183.

Batlle, E., and Massagué, J. (2019). Transforming growth factor-β signaling in immunity and cancer. Immunity *50*, 924–940.

Berenguer, J., and Celià-Terrassa, T. (2021). Cell memory of epithelial-mesenchymal plasticity in cancer. Curr. Opin. Cell Biol. *69*, 103–110.

Bhowmick, N.A., Ghiassi, M., Bakin, A., Aakre, M., Lundquist, C.A., Engel, M.E., Arteaga, C.L., and Moses, H.L. (2001). Transforming growth factor-beta1 mediates epithelial to mesenchymal transdifferentiation through a RhoA-dependent mechanism. Mol. Biol. Cell *12*, 27–36.

Bracken, C.P., and Goodall, G.J. (2022). The many regulators of epithelial-mesenchymal transition. Nat. Rev. Mol. Cell Biol. *23*, 89–90.

Chen, X., Li, Z., Yong, H., Wang, W., Wang, D., Chu, S., Li, M., Hou, P., Zheng, J., and Bai, J. (2021). Trim21-mediated HIF-1α degradation attenuates aerobic glycolysis to inhibit renal cancer tumorigenesis and metastasis. Cancer Lett. *508*, 115–126.

Chen, Y., Lu, X., Montoya-Durango, D.E., Liu, Y.H., Dean, K.C., Darling, D.S., Kaplan, H.J., Dean, D.C., Gao, L., and Liu, Y. (2017). ZEB1 regulates multiple oncogenic components involved in uveal melanoma progression. Sci. Rep. *7*, 45.

Choi, S., Kelber, J., Jiang, X., Strnadel, J., Fujimura, K., Pasillas, M., Coppinger, J., and Klemke, R. (2014). Procedures for the biochemical enrichment and proteomic analysis of the cytoskeletome. Anal. Biochem. *446*, 102–107.

Cieply, B., Farris, J., Denvir, J., Ford, H.L., and Frisch, S.M. (2013). Epithelial-mesenchymal transition and tumor suppression are controlled by a reciprocal feedback loop between ZEB1 and Grainyhead-like-2. Cancer Res. *73*, 6299–6309.

Cortes, J.R., Ambesi-Impiombato, A., Couronné, L., Quinn, S.A., Kim, C.S., da Silva Almeida, A.C., West, Z., Belver, L., Martin, M.S., Scourzic, L., et al. (2018). RHOA G17V induces T follicular helper cell specification and promotes lymphomagenesis. Cancer Cell *33*, 259–273.e7.

Delaney, M.K., Malikov, V., Chai, Q., Zhao, G., and Naghavi, M.H. (2017). Distinct functions of diaphanous-related formins regulate HIV-1 uncoating and transport. Proc. Natl. Acad. Sci. USA *114*. E6932–e6941.

Derynck, R., Turley, S.J., and Akhurst, R.J. (2021). TGFβ biology in cancer progression and immunotherapy. Nat. Rev. Clin. Oncol. *18*, 9–34.

Dongre, A., and Weinberg, R.A. (2019). New insights into the mechanisms of epithelial-mesenchymal transition and implications for cancer. Nat. Rev. Mol. Cell Biol. *20*, 69–84.

Dost, A.F.M., Moye, A.L., Vedaie, M., Tran, L.M., Fung, E., Heinze, D., Villacorta-Martin, C., Huang, J., Hekman, R., Kwan, J.H., et al. (2020). Organoids model transcriptional hallmarks of oncogenic KRAS activation in lung epithelial progenitor cells. Cell Stem Cell *27*, 663–678.e8.

Gervasi, M., Bianchi-Smiraglia, A., Cummings, M., Zheng, Q., Wang, D., Liu, S., and Bakin, A.V. (2012). JunB contributes to Id2 repression and the epithelial-mesenchymal transition in response to transforming growth factor-β. J. Cell Biol. *196*, 589–603.

Grainger, D.J., Mosedale, D.E., and Metcalfe, J.C. (2000). TGF-beta in blood: a complex problem. Cytokine Growth Factor Rev. *11*, 133–145.

Grawenda, A.M., and O'Neill, E. (2015). Clinical utility of RASSF1A methylation in human malignancies. Br. J. Cancer *113*, 372–381.

Gregory, P.A., Bert, A.G., Paterson, E.L., Barry, S.C., Tsykin, A., Farshid, G., Vadas, M.A., Khew-Goodall, Y., and Goodall, G.J. (2008). The miR-200 family and miR-205 regulate epithelial to mesenchymal transition by targeting ZEB1 and SIP1. Nat. Cell Biol. *10*, 593–601.

Guo, Y., Lu, X., Chen, Y., Rendon, B., Mitchell, R.A., Cuatrecasas, M., Cortés, M., Postigo, A., Liu, Y., and Dean, D.C. (2021). Zeb1 induces immune checkpoints to form an immunosuppressive envelope around invading cancer cells. Sci. Adv. *7*, eabd7455.

Gupta, B., Errington, A.C., Jimenez-Pascual, A., Eftychidis, V., Brabletz, S., Stemmler, M.P., Brabletz, T., Petrik, D., and Siebzehnrubl, F.A. (2021). The transcription factor ZEB1 regulates stem cell self-renewal and cell fate in the adult hippocampus. Cell Rep. *36*, 109588.

Han, Y., Villarreal-Ponce, A., Gutierrez, G., Jr., Nguyen, Q., Sun, P., Wu, T., Sui, B., Berx, G., Brabletz, T., Kessenbrock, K., et al. (2022). Coordinate control of basal epithelial cell fate and stem cell maintenance by core EMT transcription factor Zeb1. Cell Rep. *38*, 110240.

Harrell Stewart, D.R., Schmidt, M.L., Donninger, H., and Clark, G.J. (2020). The RASSF1A tumor suppressor binds the RasGAP DAB2IP and modulates RAS activation in lung cancer. Cancers *12*, E3807.

Hsu, P.C., Yang, C.T., Jablons, D.M., and You, L. (2020). The crosstalk between Src and hippo/YAP signaling pathways in non-small cell lung cancer (NSCLC). Cancers *12*, E1361.

Huang, G., Osmulski, P.A., Bouamar, H., Mahalingam, D., Lin, C.L., Liss, M.A., Kumar, A.P., Chen, C.L., Thompson, I.M., Sun, L.Z., et al. (2016). TGF-β signal rewiring sustains epithelial-mesenchymal transition of circulating tumor cells in prostate cancer xenograft hosts. Oncotarget *7*, 77124–77137.

Huang, J.J., and Blobe, G.C. (2016). Dichotomous roles of TGF-β in human cancer. Biochem. Soc. Trans. *44*, 1441–1454.

Ichikawa, K., Kubota, Y., Nakamura, T., Weng, J.S., Tomida, T., Saito, H., and Takekawa, M. (2015). MCRIP1, an ERK substrate, mediates ERK-induced gene silencing during epithelial-mesenchymal transition by regulating the co-repressor CtBP. Mol. Cell *58*, 35–46.

Jain, A.N. (2007). Surflex-Dock 2.1: Robust performance from ligand energetic modeling, ring flexibility, and knowledge-based search. J. Comput. Aided Mol. Des. *21*, 281–306.

Johnson, L., Mercer, K., Greenbaum, D., Bronson, R.T., Crowley, D., Tuveson, D.A., and Jacks, T. (2001). Somatic activation of the K-ras oncogene causes early onset lung cancer in mice. Nature *410*, 1111–1116.

Kim, T., Veronese, A., Pichiorri, F., Lee, T.J., Jeon, Y.J., Volinia, S., Pineau, P., Marchio, A., Palatini, J., Suh, S.S., et al. (2011). p53 regulates epithelial-mesenchymal transition through microRNAs targeting ZEB1 and ZEB2. J. Exp. Med. *208*, 875–883.

Kiyokawa, H., Yamaoka, A., Matsuoka, C., Tokuhara, T., Abe, T., and Morimoto, M. (2020). Airway tissue stem cells reutilize the embryonic proliferation regulator, Tgfß-Id2 axis, for tissue regeneration. Preprint at bioRxiv. https://doi.org/10.1101/2020.2011.2023.394908.

Krebs, A.M., Mitschke, J., Lasierra Losada, M., Schmalhofer, O., Boerries, M., Busch, H., Boettcher, M., Mougiakakos, D., Reichardt, W., Bronsert, P., et al. (2017). The EMT-activator Zeb1 is a key factor for cell plasticity and promotes metastasis in pancreatic cancer. Nat. Cell Biol. *19*, 518–529.

Kumar, V., Carlson, J.E., Ohgi, K.A., Edwards, T.A., Rose, D.W., Escalante, C.R., Rosenfeld, M.G., and Aggarwal, A.K. (2002). Transcription corepressor CtBP is an NAD(+)-regulated dehydrogenase. Mol. Cell *10*, 857–869.

Kuppuswamy, M., Vijayalingam, S., Zhao, L.J., Zhou, Y., Subramanian, T., Ryerse, J., and Chinnadurai, G. (2008). Role of the PLDLS-binding cleft region of CtBP1 in recruitment of core and auxiliary components of the corepressor complex. Mol. Cell Biol. *28*, 269–281.

Larsen, J.E., Nathan, V., Osborne, J.K., Farrow, R.K., Deb, D., Sullivan, J.P., Dospoy, P.D., Augustyn, A., Hight, S.K., Sato, M., et al. (2016). ZEB1 drives epithelial-to-mesenchymal transition in lung cancer. J. Clin. Invest. *126*, 3219–3235.

Lee, M.G., Jeong, S.I., Ko, K.P., Park, S.K., Ryu, B.K., Kim, I.Y., Kim, J.K., and Chi, S.G. (2016). RASSF1A directly Antagonizes RhoA activity through the assembly of a smurf1-mediated destruction complex to suppress tumorigenesis. Cancer Res. *76*, 1847–1859.

Li, J., Shen, C., Wang, X., Lai, Y., Zhou, K., Li, P., Liu, L., and Che, G. (2019). Prognostic value of TGF-β in lung cancer: systematic review and meta-analysis. BMC Cancer *19*, 691.

Liu, Y., Lu, X., Huang, L., Wang, W., Jiang, G., Dean, K.C., Clem, B., Telang, S., Jenson, A.B., Cuatrecasas, M., et al. (2014). Different thresholds of ZEB1 are required for Ras-mediated tumour initiation and metastasis. Nat. Commun. *5*, 5660.

Liu, Y., Siles, L., Lu, X., Dean, K.C., Cuatrecasas, M., Postigo, A., and Dean, D.C. (2018). Mitotic polarization of transcription factors during asymmetric division establishes fate of forming cancer cells. Nat. Commun. *9*, 2424.

Lu, W., and Kang, Y. (2019). Epithelial-mesenchymal plasticity in cancer progression and metastasis. Dev. Cell *49*, 361–374.

Lu, X., Shao, L., Qian, Y., Zhang, Y., Wang, Y., Miao, L., and Zhuang, Z. (2020). Prognostic effects of the expression of inhibitor of DNA-binding family members on patients with lung adenocarcinoma. Oncol. Lett. *20*, 143.

Lun, A.T.L., Riesenfeld, S., Andrews, T., Dao, T.P., and Gomes, T.; participants in the 1st Human Cell Atlas Jamboree (2019). EmptyDrops: distinguishing cells from empty droplets in droplet-based single-cell RNA sequencing data. Genome Biol. *20*, 63.

Lüönd, F., Pirkl, M., Hisano, M., Prestigiacomo, V., Kalathur, R.K., Beerenwinkel, N., and Christofori, G. (2022). Hierarchy of TGFβ/SMAD, Hippo/YAP/TAZ, and Wnt/β-catenin signaling in melanoma phenotype switching. Life Sci. Alliance *5*, e202101010.

Lüönd, F., Sugiyama, N., Bill, R., Bornes, L., Hager, C., Tang, F., Santacroce, N., Beisel, C., Ivanek, R., Bürglin, T., et al. (2021). Distinct contributions of partial and full EMT to breast cancer malignancy. Dev. Cell *56*, 3203–3221.e11.

Meyer-Schaller, N., Cardner, M., Diepenbruck, M., Saxena, M., Tiede, S., Lüönd, F., Ivanek, R., Beerenwinkel, N., and Christofori, G. (2019). A hierarchical regulatory landscape during the multiple stages of EMT. Dev. Cell *48*, 539–553.e6.

Monsen, R.C., and Trent, J.O. (2018). G-quadruplex virtual drug screening: a review. Biochimie *152*, 134–148.

Moroishi, T., Hansen, C.G., and Guan, K.L. (2015). The emerging roles of YAP and TAZ in cancer. Nat. Rev. Cancer *15*, 73–79.

Moustakas, A., and de Herreros, A.G. (2017). Epithelial-mesenchymal transition in cancer. Mol. Oncol. *11*, 715–717.

Nardini, M., Spanò, S., Cericola, C., Pesce, A., Massaro, A., Millo, E., Luini, A., Corda, D., and Bolognesi, M. (2003). CtBP/BARS: a dual-function protein involved in transcription co-repression and Golgi membrane fission. EMBO J. *22*, 3122–3130.

Narumiya, S., Tanji, M., and Ishizaki, T. (2009). Rho signaling, ROCK and mDia1, in transformation, metastasis and invasion. Cancer Metastasis Rev. *28*, 65–76.

Otomo, T., Otomo, C., Tomchick, D.R., Machius, M., and Rosen, M.K. (2005). Structural basis of Rho GTPase-mediated activation of the formin mDia1. Mol. Cell *18*, 273–281.

Park, J.S., Burckhardt, C.J., Lazcano, R., Solis, L.M., Isogai, T., Li, L., Chen, C.S., Gao, B., Minna, J.D., Bachoo, R., et al. (2020). Mechanical regulation of glycolysis via cytoskeleton architecture. Nature *578*, 621–626.

Pastushenko, I., Brisebarre, A., Sifrim, A., Fioramonti, M., Revenco, T., Boumahdi, S., Van Keymeulen, A., Brown, D., Moers, V., Lemaire, S., et al. (2018). Identification of the tumour transition states occurring during EMT. Nature *556*, 463–468.

Pastushenko, I., Mauri, F., Song, Y., de Cock, F., Meeusen, B., Swedlund, B., Impens, F., Van Haver, D., Opitz, M., Thery, M., et al. (2021). Fat1 deletion promotes hybrid EMT state, tumour stemness and metastasis. Nature *589*, 448–455.

Pefani, D.E., Pankova, D., Abraham, A.G., Grawenda, A.M., Vlahov, N., Scrace, S., and O' Neill, E. (2016). TGF-B targets the hippo pathway scaffold RASSF1A to facilitate YAP/SMAD2 nuclear translocation. Mol. Cell *63*, 156–166.

Postigo, A.A., and Dean, D.C. (1999). ZEB represses transcription through interaction with the corepressor CtBP. Proc. Natl. Acad. Sci. USA *96*, 6683–6688.

Postigo, A.A., Depp, J.L., Taylor, J.J., and Kroll, K.L. (2003). Regulation of Smad signaling through a differential recruitment of coactivators and corepressors by ZEB proteins. EMBO J. *22*, 2453–2462.

Rana, M.K., Aloisio, F.M., Choi, C., and Barber, D.L. (2018). Formin-dependent TGF-β signaling for epithelial to mesenchymal transition. Mol. Biol. Cell *29*, 1465–1475.

Rawlins, E.L., Clark, C.P., Xue, Y., and Hogan, B.L.M. (2009). The Id2+ distal tip lung epithelium contains individual multipotent embryonic progenitor cells. Development *136*, 3741–3745.

Saito, Y., Yuki, H., Kuratani, M., Hashizume, Y., Takagi, S., Honma, T., Tanaka, A., Shirouzu, M., Mikuni, J., Handa, N., et al. (2013). A pyrrolo-pyrimidine derivative targets human primary AML stem cells in vivo. Sci. Transl. Med. *5*, 181ra52.

Santos, C.P., Lapi, E., Martínez de Villarreal, J., Álvaro-Espinosa, L., Fernández-Barral, A., Barbáchano, A., Domínguez, O., Laughney, A.M., Megías, D., Muñoz, A., and Real, F.X. (2019). Urothelial organoids originating from Cd49f(high) mouse stem cells display Notch-dependent differentiation capacity. Nat. Commun. *10*, 4407.

Schmidt, M.L., Hobbing, K.R., Donninger, H., and Clark, G.J. (2018). RASSF1A deficiency enhances RAS-driven lung tumorigenesis. Cancer Res. *78*, 2614–2623.

Shreberk-Shaked, M., and Oren, M. (2019). New insights into YAP/TAZ nucleo-cytoplasmic shuttling: new cancer therapeutic opportunities? Mol. Oncol. *13*, 1335–1341.

Tehrani, S., Tomasevic, N., Weed, S., Sakowicz, R., and Cooper, J.A. (2007). Src phosphorylation of cortactin enhances actin assembly. Proc. Natl. Acad. Sci. USA *104*, 11933–11938.

Varma, S., Cao, Y., Tagne, J.B., Lakshminarayanan, M., Li, J., Friedman, T.B., Morell, R.J., Warburton, D., Kotton, D.N., and Ramirez, M.I. (2012). The transcription factors Grainyhead-like 2 and NK2-homeobox 1 form a regulatory loop that coordinates lung epithelial cell morphogenesis and differentiation. J. Biol. Chem. *287*, 37282–37295.

Vlahov, N., Scrace, S., Soto, M.S., Grawenda, A.M., Bradley, L., Pankova, D., Papaspyropoulos, A., Yee, K.S., Buffa, F., Goding, C.R., et al. (2015). Alternate RASSF1 transcripts control SRC activity, E-cadherin contacts, and YAP-mediated invasion. Curr. Biol. *25*, 3019–3034.

Wang, J., Scully, K., Zhu, X., Cai, L., Zhang, J., Prefontaine, G.G., Krones, A., Ohgi, K.A., Zhu, P., Garcia-Bassets, I., et al. (2007). Opposing LSD1 complexes function in developmental gene activation and repression programmes. Nature *446*, 882–887.

Wang, L., Wang, S., Shi, Y., Li, R., Günther, S., Ong, Y.T., Potente, M., Yuan, Z., Liu, E., and Offermanns, S. (2020). YAP and TAZ protect against white adipocyte cell death during obesity. Nat. Commun. *11*, 5455.

Wellner, U., Schubert, J., Burk, U.C., Schmalhofer, O., Zhu, F., Sonntag, A., Waldvogel, B., Vannier, C., Darling, D., zur Hausen, A., et al. (2009). The EMT-activator ZEB1 promotes tumorigenicity by repressing stemness-inhibiting microRNAs. Nat. Cell Biol. *11*, 1487–1495.

Yang, Y., Ahn, Y.H., Chen, Y., Tan, X., Guo, L., Gibbons, D.L., Ungewiss, C., Peng, D.H., Liu, X., Lin, S.H., et al. (2014). ZEB1 sensitizes lung adenocarcinoma to metastasis suppression by PI3K antagonism. J. Clin. Invest. *124*, 2696–2708.

Zhang, C., Zhu, H., Ren, X., Gao, B., Cheng, B., Liu, S., Sha, B., Li, Z., Zhang, Z., Lv, Y., et al. (2021). Mechanics-driven nuclear localization of YAP can be reversed by N-cadherin ligation in mesenchymal stem cells. Nat. Commun. *12*, 6229.

Zhang, Q., Piston, D.W., and Goodman, R.H. (2002). Regulation of corepressor function by nuclear NADH. Science *295*, 1895–1897.

Zhang, Y., and Weinberg, R.A. (2018). Epithelial-to-mesenchymal transition in cancer: complexity and opportunities. Front. Med. *12*, 361–373.

Zhao, L.J., Kuppuswamy, M., Vijayalingam, S., and Chinnadurai, G. (2009). Interaction of ZEB and histone deacetylase with the PLDLS-binding cleft region of monomeric C-terminal binding protein 2. BMC Mol. Biol. *10*, 89.

STAR★METHODS

KEY RESOURCES TABLE

REAGENT or RESOURCE	SOURCE	IDENTIFIER
Antibodies		
Vimentin	Santa Cruz	Sc-7557;RRID:AB_793998
e-cadherin	BD Biosciences Lab	610181;RRID:AB_397580
Tgfb1	Santa cruz	Sc-146;RRID:AB_632486
Yap1	Cell signaling	4912;RRID:AB_2218911
Zeb1	Douglas darling	Gift
CtBP (E-12)	Santa cruz	Sc-17759;RRID:AB_11150115
coRest(H-8)	Santa cruz	Sc-376567;RRID:AB_2182605
RhoA	Cytoskeleton	Arh04;RRID:AB_2728698
RhoA (1A11-4G10)	Novus	NBP2-22528;RRID:AB_1217817
ACTB	Sigma	A1978;RRID:AB_476692
HDAC2 (3F3)	Santa cruz	Sc-81599;RRID:AB_2118560
mDia1	proteintech	20624-1-ap;RRID:AB_10858618
Chemicals, peptides, and recombinant proteins		
C3 transferase	Cytoskeleton inc	Ct03-a
Y27632 (Tocris)	sigma	1254
SMIFH2	sigma	S4826
A-419259	R&d systems	1435934-25-0
Critical commercial assays		
Proteoextract	sigma	17-10195
ChIP kit	qiagen	Gah-2206
Trizo RNA extraction kit	Invitrogen	15596026
RT kit	Invitrogen	12594025
CtBP1 lentivirus knockdown CtBP2 lentivirus knockdown	Santa cruz Santa cruz	sc-35121-SH sc-37768-SH
Deposited data		
Human LUAD samples	NCBI database	GSE_11969
Human LUAD scRNAseq data	Expression Omnibus	GSE149655
Experimental models: Cell lines		
393P primary mouse LUAD	Jon Kurie	gift
NCL-H1437 human LUAD	Harrell Stewart et al., 2020	Geoff Clark
Experimental models: Organisms/strains		
LA1 mice	Jackson labs	N/A
Rassf1a mutant mice	Schmidt et al., 2018	Geoff Clark

RESOURCE AVAILABILITY

Lead contact

Further information and requests for resources and reagents should be directed to and will be fulfilled by the lead contact, Douglas Dean (douglas.dean@louisville.edu).

Materials availability

Antibodies and chemical sources are presented in the Key resources Table.

Data and code availability

This paper analyzes existing, publicly available data. These accession numbers for the datasets are listed in the key resources table. All other data reported in this paper will be shared by the lead contact upon request.

This paper does not report original code. Any additional information required to reanalyze the data reported in this paper is available from the lead contact upon request.

EXPERIMENTAL MODEL AND SUBJECT DETAILS

Mice

Housing and handling of all mice was in accordance with procedures approved by the University of Louisville Institutional Animal Care and Use Committee (IACUC). K-ras^{LA1} mice (Johnson et al., 2001) in a C57BL/6 background were obtained from Jackson Laboratory. Mice expressing doxycycline-inducible *K-Ras4b* ^{G12D} in lung ATII cells and *Rassf1a* knockout mice, both in a C57/BL6 background were described previously (Schmidt et al., 2018). Animals of approximately four months of age were induced by feeding doxycycline chow (Harlan's Telklad 200 mg/kg doxycycline food) for three months (Schmidt et al., 2018). Tumor pathology was evaluated blindly by an experienced pathologist (MC). Based on our previous studies, we did not detect differences with regard to sex, thus male and female mice were chosen at random.

Human studies

Human LUDA scRNASeq

A description of the cell capture, sequencing, and read alignment for the human LUAD samples were described previously (Dost et al., 2020). The current analysis was performed using the 10X Genomics Cloupe Browser 5.0 (10X Genomics, Pleasanton, CA), which allows for interactive visualization and analysis. For each sample, a feature-barcode matrix containing read counts for each gene across all cells was retrieved from the Gene Expression Omnibus (GSE149655) and converted to a Cloupe format for input to the browser. To create the Cloupe files, each matrix was converted to HDF5 format using the write10xCounts function from the DropletUtils R package (Lun et al., 2019). The HDF5 file was converted to a Cloupe file using the 10X Genomics Cell Ranger reanalyze function.

Samples from two patients with radiographic diagnosis of stage IA LUAD were analyzed in these studies (Dost et al., 2020). One patient was female, 74 years old, with a KRAS-G12F mutation identified as driver mutation. The other patient was female, 77 years old, with a KRAS-G12V mutation identified as driver mutation.

Human K-Ras mutant LUAD

Formalin-fixed, paraffin-embedded sections of human LUAD were obtained from IDIBAPS' Tumor Bank and their use was approved by the ethics committee. These samples were sequenced for both *K-Ras* and *EGFR* mutations, as we described previously (Liu et al., 2014).

Cell lines, primary culture

When mouse K-Ras initiated lung tumors were dissociated and placed in culture, a subset of tumor cells survived and proliferated, and these cells were highly tumorigenic when delivered intratracheally back into wild-type lungs (Ahn et al., 2012; Liu et al., 2018). These cells were grown in DMEM with 10% heat-inactivated fetal bovine serum. Human lung tumor cells were cultured as described previously (Harrell Stewart et al., 2020).

METHOD DETAILS

Cell fractionation

Cells were fractionated into cytoskeleton, soluble cytoplasm and nucleus using a ProteoExtract cytoskeleton enrichment kit (Sigma #17-10195) as described previously (Choi et al., 2014). Cells grown to 70%–80% confluency in 150 mm were placed on ice. After removal of the culture medium, 5 mL of cold phosphate buffered saline (PBS) was used to wash the cells twice. Next, 5 mL of ice-cold cell lysis buffer (50 mM PIPES, 50 mM NaCl, 5% Glycerol, 0.1% NP-40, 0.1% Triton X-100 and 0.1% Tween 20) was added to the dish and kept on ice for 1.5 min. Lysates were collected and kept on ice for further use. The cells were further rinsed gently with 5 mL Tris-HCl buffer (50 mM Tris-HCl, pH 7.5) and incubated with 5 mL of Nuclease buffer [10 U/mL Benzoase nuclease (Sigma-Aldrich), 10 mM $MgCl_2$ and 2 mM $CaCl_2$ in 50 mM Tris-HCl buffer, pH 7.5] for 10 min at room temperature. After removal of the Nuclease buffer, aliquots of the previously collected lysates (in lysis buffer) were added to release and solubilize the DNA or RNA binding proteins for another 30 s on ice. Cytoskeletal proteins remaining bound to the dish were then rinsed using 5 mL of cold Tris-HCl buffer three times on ice, and solubilized/denatured in 500 μL of 1% SDS. The total protein concentration was determined using the BCA protein assay (Pierce). All the buffers used during the cytoskeleton extraction procedure contained protease (Roche protease inhibitor cocktail) and phosphatase inhibitors (5 mM NaF, 2 mM sodium vanadate and 10 mM β-glycerophosphate).

F actin number and length

Phalloidin staining was used to identify F actin polymers. The number of polymers was counted in the x-y and z dimensions of merged confocal z stacks in 20× microscopic views of fifty confluent cells. Polymer length in the x-y and z dimensions was measured in single

cells by switching to a high power 40X view. Confluent cells on tissue culture plates were approximately 15 μm in thickness (z-dimension).

RhoA, Formin, Src and ROCK inhibition

Cell-permeable c3 transferase (Cytoskeleton Inc.) was used at 1 ug/mL to inhibit RhoA (Wang et al., 2020). and SMIFH2 (Sigma) were used at 5 μm to inhibit ROCK and Formins, respectively (Delaney et al., 2017; Santos et al., 2019) A-419259 (R&D Systems) was used at 0.5 μm to inhibit Src (Saito et al., 2013). Cells were analyzed after 6 hrs of treatment.

RNA extraction, real-time PCR and ChIP assays

RNA was extracted using TRIzol (Invitrogen, Carlsbad, CA). cDNA was synthesized using the Invitrogen RT Kit according to the manufacturer's protocol (Invitrogen). Real-time quantitative PCR was performed using the Mx3000P Real-Time PCR System (Stratagene, Cedar Creek, TX) according to the manufacturer's instructions. PCR primers are shown in Table S3. Three independent samples, each in triplicate, were analyzed for each real-time PCR condition, and products were analyzed for size by agarose gel.

Chromatin immunoprecipitation (ChIP) assays used a kit (Qiagen, Cat# GAH-2206). Formaldehyde was used to cross-link genomic DNA. The chromatin polyclonal antiserum for Zeb1 was used for immunoprecipitation whereas equal amount of pre-immune serum was used as a control (IgG). Immunoprecipitation with histone 3 antibody (H3) included in the ChIP antibody kit was used as a positive control. Sequences of primers for the *Rassf1a* promoter and the expected sizes of the PCR products are shown in Figure 4F and Table S3. ChIP-PCR programs were similar to that described for qPCR, but with additional 1% BSA and 1% DMSO, and the PCR program had a higher annealing temperature (e.g. 60–68°C) and longer extension time (1 min). Results are representative of three independent experiments.

shRNA knockdown

We have previously described lentiviral shRNA knockdown of Zeb1 (Liu et al., 2014). To generate a lentivirus expressing ZEB1 shRNA, a primer containing a ZEB1 shRNA sequence (5′-CTGTCTAGACAAAAAAAGACAACGTGAAAGACAATCTCTTGAATTGTCAAA CACGTTGTCTTGGGGATCTGTGGTCTCATACA-3′) was used with a T3 primer to amplify a 500-base-pair fragment containing the H1 promoter using the pSuper vector as a template. The resulting PCR product was digested with SpeI and XbaI and cloned back into the lentiviral vector digested with NheI. We first cloned the shRNA sequence into a CMV-GFP lentiviral vector, where its expression was driven by the mouse U6 promoter. Briefly, the shRNA construct was generated by synthesizing an 83-mer oligonucleotide containing: (i) a 19-nucleotide sense strand and a 19-nucleotide antisense strand, separated by a nine-nucleotide loop (5′-TTCAAGAGA-3′); (ii) a stretch of five adenines as a template for the Pol III promoter termination signal; (iii) 21 nucleotides complementary to the 3′ end of the *Pol III* U6 promoter; and (iv) a 5′ end containing a unique XbaI restriction site. The long oligonucleotide was used, together with an sp6 oligonucleotide (5′-ATTTAGGTGACACTATAGAAT-3′), to PCR amplify a fragment containing the entire U6 promoter plus shRNA sequences; the resultant product was digested with XbaI and SpeI ligated into the NheI of the lentivirus vector, and the insert was sequenced to ensure that no errors occurred during the PCR or cloning steps. Lentiviral particles were produced by a four-plasmid transfection system. Briefly, 293T cells were transfected with the lentiviral vector and packaging plasmids, and the supernatants, containing recombinant pseudolentiviral particles, were collected from culture dishes on the second and third days after transfection. TKO MEFs and Ras-TKO MEFs were transduced with these lentiviral particles expressing shRNAs targeting ZEB1. Beyond this original shRNA, we used five additional shRNA lentiviruses with different ZEB1 shRNA sequences from Open Biosystems for knockdowns with similar effects. Lentivirus with a scrambled shRNA sequence 5′-CAACAAGATGAAGAGCACCAATCTCTTGAATTGGTGCTCTT CATCTTGTTG-3′ was used as a control—this control sequence was blasted against all mouse RNA sequences to insure that it did not target an mRNA. For RASSF1A shRNA knockdown (Harrell Stewart et al., 2020; Schmidt et al., 2018), An shRNA expression cassette containing the hairpin sequence, ATGAAGCCGCCACAGAGGCCACACCACATCCAAACGTGGTGCGACCTCTGTGGC GACTTCAT, was cloned in the pSHAG-MAGIC1 (pSM2) vector. H1792 cells were transfected with 1–5 μg of shRNA vector and selected in puromycin. Selected cells were examined for loss of RASSF1A expression by Western analysis using a RASSF1A polyclonal antibody and by qRT-PCR. qRT-PCR. For knockdown of CtBP1 and 2, a mixture of 3 CtBP1 (Santa Cruz Biotechnology, cat. #: sc-35121-SH) and 3 CtBP 2 shRNA lentiviral vectors with puromycin selection (Santa Cruz Biotechnology, cat. #: sc-37768-SH) were transfected using Lipofectamin3000 (Invitrogen, cat. #: L3000-015) according to the manufacturer's instruction into 293T cells to generate lentiviral particles. Briefly, 293T cells were cultured until 70-80% confluence when the mixture of lentiviral package plasmids (pMDLg/pRRE, pRSV.Rev and pMD2.G at ratio of 1:1:1) was combined with the above CtBP 1 and 2 shRNA lentiviral vectors at 1:1 ratio. OPTI-MEM and lipofectamin3000 were sequentially added into a tube containing the above plasmids. The mixture was then added to the 293T cells cultured in DMEM with 10% fetal bovine serum. Two days later medium containing lentivirus particles was harvested. Primary mouse LUAD cells were infected with 200 μL of media and selected with 5μg/mL puromycin for 2 days.

Immunostaining

Immunostaining of LUAD was describe in detail previously (Liu et al., 2014). Tissue collection and cell preparation, and immunostaining was performed by different lab members. Briefly, slides were washed with PBS, fixed with 4% formaldehyde for 10 min, and then washed again with PBS and treated with methanol at −20°C for 10 minutes, and blocked with 4% goat at room temperature for one hr. Slides were incubated with primary antibody overnight at 4°C. The next day, slides were washed with PBS followed by incubation

with secondary antibody for 1 hr at room temperature. Antibodies for immunostaining are described in Table S4. Fluorescent images were captured using an Olympus FV300 confocal microscope (Olympus Confocal America, Inc., Center Valley, PA). Images shown are maximum projections of confocal stacks, adjusted for contrast and brightness with Adobe Photoshop Elements v9.0.2 (Adobe Systems, Inc., San Jose, CA) and transferred to Powerpoint for figure assembly. As a negative control, no immunostaining was evident in the absence of primary antibodies.

Identification of a novel Zeb1-CtBP binding inhibitor

The crystal structure of the PLDLS:CtBP complex was used in virtual screens of the ZINC 2014 drug-like library (24,877,119 compounds) with Surflex-Dock (Jain, 2007), as we described (Monsen and Trent, 2018). The library is prefiltered for drug-like properties by Lipinski's rules. The PLDLSKK peptide from 1HL3 was used to generate a protomol as initial search locations for Surflex-Dock screening. Due to sufficient available resources, we routinely screen at the highest level (-pgeom) with pre- and post-minimization. This screen resulted in 27 compounds with appropriate predicted affinity constants (-logK_d >12 for Surflex-Dock). These compounds were then screened for solubility and their ability to inhibit Zeb1-dependent functions in cell culture and CtBP binding in Co-IP assays. Results with one of these compounds is shown in Figures 2 and S1.

Characterization of a RASSF1A, ID2 signature in human LUAD

Expression data for human LUAD sequenced for mutations in K-RAS and EGFR mutations and patient-matched control lung tissue were obtained from the NCBI database (GSE_11969). Data were corrected for background and normalized to median fluorescence and GAPDH mRNA expression. GO analysis was performed using DAVID Gene Ontology https://david.ncifcrf.gov/.

QUANTIFICATION AND STATISTICAL ANALYSIS

Statistical testing was performed using GraphPad Prism. p values are indicated in the figures, and p values <0.05 were considered significant.